Supporting Information for

Sensitive Detection of Formaldehyde via a Luminescent Distorted Eu_4L_4 Tetrahedral Cage

Ran Li,[ab] Xuan Deng,[ab] Fan Yin,[b] Xiao-Fang Duan,[b] Li-Peng Zhou,[b] Yang Zhou,[b] Xiao-Qing Guo*[b] and Qing-Fu Sun*[ab]

a. College of Chemistry, Fuzhou University, Fuzhou 350108, People's Republic of China.
b. Fujian College, University of Chinese Academy of Sciences, Fuzhou 350002, People's Republic of China.
*Correspondence to: guoxiaoqing@fjirsm.ac.cn, qfsun@fjirsm.ac.cn.

Contents

1. General

Unless otherwise specified, all chemicals and solvents were obtained from commercial companies and used without further purification. Deuterated solvents were purchased from Admas and Cambridge Isotope Labs. 1D and 2D-NMR spectra were acquired using Bruker Biospin Avance III (400 MHz), JEOL ECZ400S (400 MHz), and JEOL ECZ600S (600 MHz) spectrometers. Chemical shifts in ^{1}H-NMR were referenced to TMS or the residual signals of the deuterated solvents used. ESI-TOF-MS was conducted on a Bruker Impact II UHR-TOF mass spectrometry, with a tuning mix serving as the internal standard. Data analysis was conducted with Bruker Data Analysis software (Version 4.3), and simulations were executed using Bruker Isotope Pattern software. UV-vis spectra were recorded with a SHIMADZU UV-2700 spectrophotometer. Luminescence spectra were measured using an FS5 spectrofluorometer from Edinburgh Photonics, with spectra corrected for experimental functions. SEM images were obtained with Thermofisher Scientific Apreo 2S HiVac. AFM images were obtained with Bruker Dimension Icon. The thickness of film was measured with Bruker Dektak-XT. X-ray crystal data were collected on Rigaku Synergy-S (Cu - Kα radiation: λ = 1.54184 Å) and micro-focus metaljet diffractometer (Ga Kα radiation λ = 1.3405 Å)

2. Experimental Details

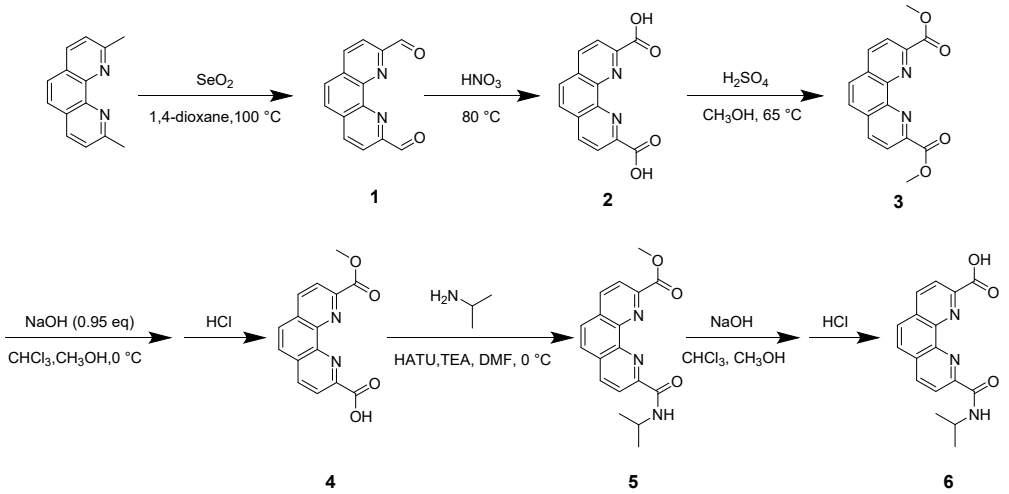

Scheme S1. Synthetic route of compound **6**.

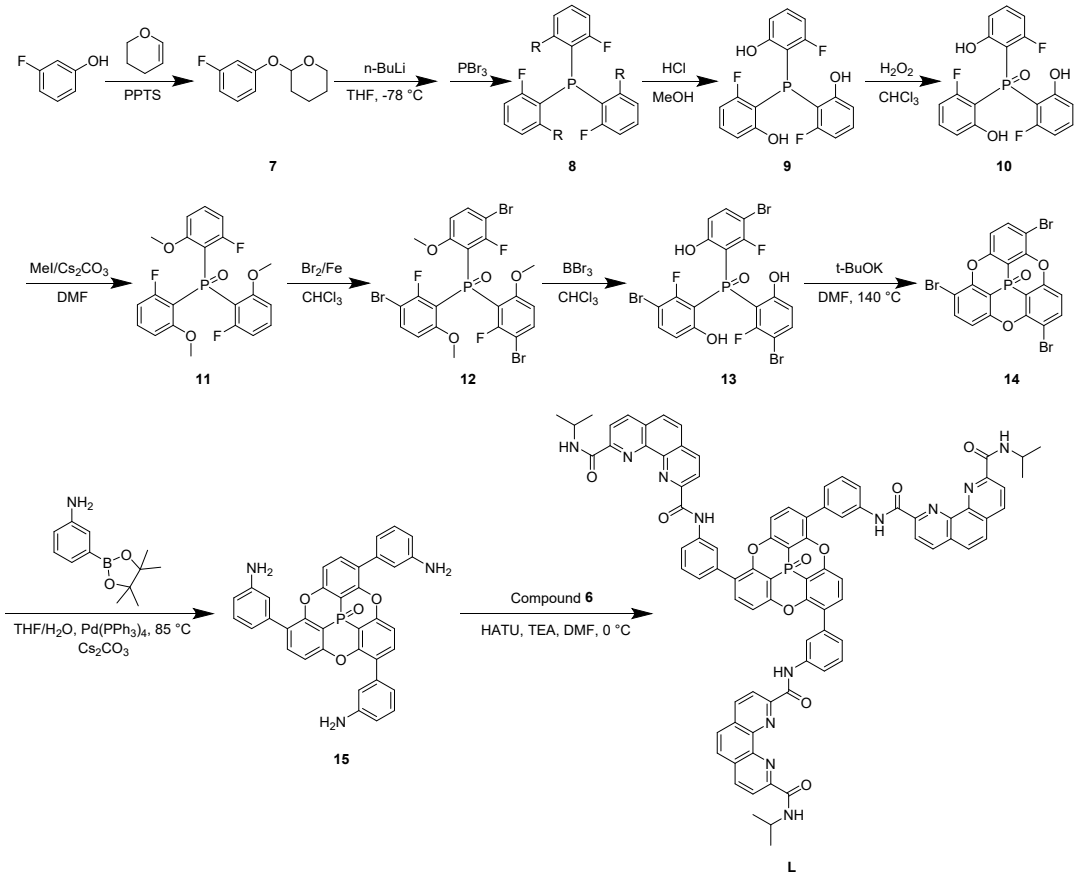

Scheme S2. Synthetic route of the ligand **L**.

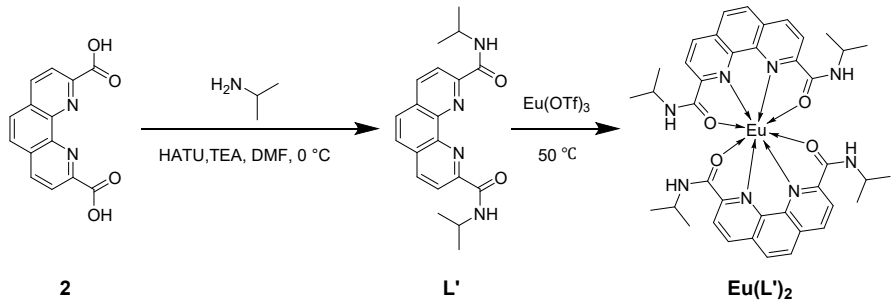

Scheme S3. Synthetic route of the ligand **L'** and **Eu(L')$_2$**.

Compounds **1**-**6** and **7**-**14** were synthesized according to established literature procedures. [S1-S3]

Synthesis of compound 15

To a solution of THF/H_2O (3:1, 210 mL), compound **14** (591 mg, 1.06 mmol, 1.0 equiv) was added, along with 3-aminophenylboronic acid pinacol ester (929 mg, 4.24 mmol, 4.0 equiv), $Pd(PPh_3)_4$ (244 mg, 0.21 mmol, 0.2 equiv), and Cs_2CO_3 (1.04 g, 3.18 mmol, 3.0 equiv). The mixture was degassed under nitrogen for 30 minutes and then heated at 85 °C for 72 hours under a nitrogen atmosphere. After cooling to room temperature, the reaction mixture was extracted three times with 120 mL of dichloromethane. The combined organic layers were washed with brine, dried over Na_2SO_4, and concentrated under reduced pressure. The crude product was purified by column chromatography (SiO_2, DCM/MeOH = 100/1) to afford compound **15** as a pale yellow solid (585 mg, 93%). ^{1}H NMR (400 MHz, DMSO-d_6) δ = 7.66 (d, J = 8.6 Hz), 7.40 (dd, J = 8.5, 4.7 Hz), 7.17 (t, J = 7.8 Hz), 6.84 (s), 6.74 (d, J = 7.6 Hz), 6.65 (d, J = 8.0 Hz), 5.28 (s). ^{13}C NMR (101 MHz, DMSO-d_6) δ = 158.2, 155.4, 149.0, 135.3, 129.7, 129.4, 116.8, 115.9, 114.6, 113.9, 110.9, 109.8. ^{31}P NMR (243 MHz, DMSO-d_6) δ = 46.77 (s). ESI-TOF-MS for $C_{36}H_{24}N_3O_4P$ $[M + Na]^+$: calcd, m/z = 616.1397; found 616.1399.

Synthesis of ligand L

Compound **6** (155 mg, 0.502 mmol, 3.3 equiv), compound **15** (90 mg, 0.152 mmol, 1.0 equiv), and DMF (50 mL) were added into a 100 mL one-necked flask. After cooling the mixture in an ice bath, HATU/2-(7-aza-1H-benzotriazole-1-yl)-1,1,3,3-

tetramethyluronium (347 mg, 0.912 mmol, 6.0 equiv) and Et_3N (1 mL) were added, and the reaction mixture was stirred for 16 hours. The solvent was then removed under reduced pressure, and the crude product was extracted three times with dichloromethane and water. The combined organic phases were dried over Na_2SO_4, and the solvent was removed under reduced pressure. The crude product was purified by column chromatography (SiO_2, DCM/MeOH = 50/1), yielding ligand **L** as a white solid. (181 mg, 81%). ^{1}H NMR (400 MHz, $CDCl_3$) δ = 10.80 (s, 1H), 8.71 (d, *J* = 8.2 Hz, 1H), 8.62 (d, *J* = 8.2 Hz, 1H), 8.52 (d, *J* = 8.3 Hz, 1H), 8.46 (d, *J* = 8.2 Hz, 2H), 8.39 (s, 1H), 7.96 (s, 2H), 7.81 (d, *J* = 7.8 Hz, 1H), 7.68 (d, *J* = 8.6 Hz, 1H), 7.58 (t, *J* = 7.8 Hz, 1H), 7.43 (t, *J* = 8.7 Hz, 2H), 4.41 (dd, *J* = 13.8, 6.8 Hz, 1H), 1.40 (dd, *J* = 15.4, 6.5 Hz, 5H). ^{13}C NMR (101 MHz, $CDCl_3$) δ = 163.3, 162.0, 159.4, 156.1, 150.2, 149.4, 144.0, 138.2, 138.1, 137.9, 136.6, 134.8, 130.8, 130.6, 129.2, 128.2, 127.6, 125.8, 121.8, 121.5, 120.4, 119.1, 115.7, 41.8, 23.0. ^{31}P NMR (162 MHz, $CDCl_3$) δ = 47.42 (s). ESI-TOF-MS for $C_{87}H_{63}N_{12}O_{10}P$ $[M + H]^+$: calcd, m/z = 1468.4632; found 1468.4549.

Synthesis of $Eu_4L_4(OTf)_{12}$

To a suspension of **L** (2.00 mg, 1.36 μmol) in 600 μL of a mixed acetonitrile and methanol solvent (v/v = 2/1), $Eu(OTf)_3$ (0.82 mg, 1.36 μmol) was added. The mixture was stirred at 50 ℃ for approximately one hour, during which the turbid suspension gradually transformed into a homogenous yellow solution. ^{31}P NMR (162 MHz, CD_3CN/CD_3OD v/v = 2/1) δ = -160.41 (s). ESI-TOF-MS for $Eu_4\mathbf{L}_4(OTf)_{12}$: calcd for $[Eu_4\mathbf{L}_4(OTf)_0\text{-}4(HOTf)]^{8+}$ 809.1837, found 809.1628; calcd for $[Eu_4\mathbf{L}_4(OTf)_0\text{-}5(HOTf)]^{7+}$ 924.7808, found 924.7561; calcd for $[Eu_4\mathbf{L}_4(OTf)_1\text{-}4(HOTf)]^{7+}$ 946.2036, found 946.1788; calcd for $[Eu_4\mathbf{L}_4(OTf)_0\text{-}6(HOTf)]^{6+}$ 1078.5758, found 1078.5477; calcd for $[Eu_4\mathbf{L}_4(OTf)_1\text{-}5(HOTf)]^{6+}$ 1103.5691, found 1103.5402; calcd for $[Eu_4\mathbf{L}_4(OTf)_2\text{-}4(HOTf)]^{6+}$ 1128.5623, found 1128.5333; calcd for $[Eu_4\mathbf{L}_4(OTf)_3\text{-}3(HOTf)]^{6+}$ 1153.5556, found 1153.5262; calcd for $[Eu_4\mathbf{L}_4(OTf)_0\text{-}7(HOTf)]^{5+}$ 1294.2892, found 1294.2555; calcd for $[Eu_4\mathbf{L}_4(OTf)_1\text{-}6(HOTf)]^{5+}$ 1324.2827, found 1324.2477; calcd for $[Eu_4\mathbf{L}_4(OTf)_2\text{-}5(HOTf)]^{5+}$ 1354.2737, found 1354.2342; calcd for

$[Eu_4\mathbf{L}_4(OTf)_3\text{-}4(HOTf)]^{5+}$ 1354.2651, found 1354.2297; calcd for $[Eu_4\mathbf{L}_4(OTf)_4\text{-}3(HOTf)]^{5+}$ 1414.2575, found 1414.2208; calcd for $[Eu_4\mathbf{L}_4(OTf)_0\text{-}8(HOTf)]^{4+}$ 1617.3597, found 1617.3178; calcd for $[Eu_4\mathbf{L}_4(OTf)_1\text{-}7(HOTf)]^{4+}$ 1654.8500 found 1654.8046; calcd for $[Eu_4\mathbf{L}_4(OTf)_2\text{-}6(HOTf)]^{4+}$ 1692.3386 found 1692.2949; calcd for $[Eu_4\mathbf{L}_4(OTf)_3\text{-}5(HOTf)]^{4+}$ 1729.8298 found 1729.7842; calcd for $[Eu_4\mathbf{L}_4(OTf)_4\text{-}4(HOTf)]^{4+}$ 1767.3197 found 1767.2756; calcd for $[Eu_4\mathbf{L}_4(OTf)_5\text{-}3(HOTf)]^{4+}$ 1804.8090 found 1804.7627. Elemental analyses calcd (%) for $C_{360}H_{252}Eu_4N_{48}O_{76}F_{36}P_4S_{12}$: C, 52.3; H, 3.1; N, 8.1; S, 4.7; Found: C, 52.0; H, 3.2; N, 7.5; S, 4.4.

Synthesis of $Gd_4L_4(OTf)_{12}$

To a suspension of **L** (2.00 mg, 1.36 μmol) in 600 μL of a mixed acetonitrile and methanol solvent (v/v = 2/1), $Gd(OTf)_3$ (0.82 mg, 1.36 μmol) was added. The mixture was stirred at 50 ℃ for approximately one hour, during which the turbid suspension gradually transformed into a homogenous yellow solution. ESI-TOF-MS for $Gd_4\mathbf{L}_4(OTf)_{12}$: calcd for $[Gd_4\mathbf{L}_4(OTf)_0\text{-}4(HOTf)]^{8+}$ 811.9356, found 811.9338; calcd for $[Gd_4\mathbf{L}_4(OTf)_1\text{-}3(HOTf)]^{8+}$ 830.4302, found 830.4284; calcd for $[Gd_4\mathbf{L}_4(OTf)_0\text{-}5(HOTf)]^{7+}$ 927.6394, found 927.6369; calcd for $[Gd_4\mathbf{L}_4(OTf)_1\text{-}4(HOTf)]^{7+}$ 949.0622, found 949.0595; calcd for $[Gd_4\mathbf{L}_4(OTf)_2\text{-}3(HOTf)]^{7+}$ 970.4850, found 970.4807; calcd for $[Gd_4\mathbf{L}_4(OTf)_0\text{-}6(HOTf)]^{6+}$ 1082.0781, found 1082.0744; calcd for $[Gd_4\mathbf{L}_4(OTf)_1\text{-}5(HOTf)]^{6+}$ 1107.0714, found 1107.0677; calcd for $[Gd_4\mathbf{L}_4(OTf)_2\text{-}4(HOTf)]^{6+}$ 1132.2315, found 1132.2273; calcd for $[Gd_4\mathbf{L}_4(OTf)_0\text{-}7(HOTf)]^{5+}$ 1298.2923, found 1298.2829; calcd for $[Gd_4\mathbf{L}_4(OTf)_1\text{-}6(HOTf)]^{5+}$ 1328.2842, found 1328.2791; calcd for $[Gd_4\mathbf{L}_4(OTf)_2\text{-}5(HOTf)]^{5+}$ 1358.2761, found 1358.2718; calcd for $[Gd_4\mathbf{L}_4(OTf)_3\text{-}4(HOTf)]^{5+}$ 1388.2680, found 1388.2641; calcd for $[Gd_4\mathbf{L}_4(OTf)_4\text{-}3(HOTf)]^{5+}$ 1418.2608, found 1418.2578; calcd for $[Gd_4\mathbf{L}_4(OTf)_0\text{-}8(HOTf)]^{4+}$ 1622.6135, found 1622.6006; calcd for $[Gd_4\mathbf{L}_4(OTf)_2\text{-}6(HOTf)]^{4+}$ 1696.5933, found 16967.5860; calcd for $[Gd_4\mathbf{L}_4(OTf)_3\text{-}5(HOTf)]^{4+}$ 1735.3336, found 1735.3283; calcd for $[Gd_4\mathbf{L}_4(OTf)_4\text{-}4(HOTf)]^{4+}$ 1772.3228, found 1772.3171.

Synthesis of compound L'

Compound **2** (2.4 g, 8.96 mmol, 1.0 equiv), isopropylamine (1.6 g, 26.7 mmol, 3.0 equiv), and DMF (300 mL) were added into a 500 mL one-necked flask. After cooling the mixture in an ice bath, HATU/2-(7-aza-1H-benzotriazole-1-yl)-1,1,3,3-tetramethyluronium (13.6 g, 35.8 mmol, 4.0 equiv) and Et_3N (3 mL) were added, and the reaction mixture was stirred for 16 hours. The solvent was then removed under reduced pressure, and the crude product was washed with cyclohexane before extracting three times with dichloromethane and water. The combined organic phases were dried over Na_2SO_4, and the solvent was removed under reduced pressure. The crude product was purified by column chromatography (SiO_2, DCM/MeOH = 100/1), yielding compound **L'** as a white solid. (1.5 g, 47%). ^{1}H NMR (600 MHz, $CDCl_3$) δ = 8.60 (d, *J* = 8.2 Hz), 8.48 (d, *J* = 7.8 Hz), 8.45 (d, *J* = 8.2 Hz), 7.93 (s), 4.42 (dhept, *J* = 19.8, 6.6 Hz), 1.43 (d, *J* = 6.6 Hz). ^{13}C NMR (151 MHz, $CDCl_3$) δ = 163.48 (s), 150.08 (s), 144.14 (s), 137.93 (s), 130.56 (s), 127.82 (s), 121.60 (s), 41.79 (s), 23.12 (s).

Synthesis of mononuclear complex Eu(L')$_2$(OTf)$_3$

To a solution of **L'** (3.5 mg, 1.0 μmol) in 600 μL of a mixed acetonitrile and methanol solvent (v/v = 2/1), $Eu(OTf)_3$ (3.0 mg, 0.5 μmol) was added, then the mixture was stirred at 50 ℃ for approximately one hour. ^{1}H NMR (600 MHz, CD_3CN/CD_3OD v/v = 2/1) δ = 6.78 (d, *J* = 8.5 Hz), 6.67 (s), 6.22 – 5.97 (m), 3.53 (s), 1.10 (d, *J* = 6.1 Hz). ^{13}C NMR (151 MHz, CD_3CN/CD_3OD v/v = 2/1) δ = 149.05 (s), 124.81 (s), 109.03 (s), 92.45 (s), 44.36 (s), 23.10 (s), 20.46 (s). ESI-TOF-MS for Eu(**L'**)$_2$(OTf)$_3$: calcd for $[Eu(\mathbf{L'})_2(OTf)_1]^{2+}$ 501.1105, found 501.1104; calcd for $[Eu(\mathbf{L'})_2(OTf)_2]^{+}$ 1151.1734, found 1151.1731.

Eu(6)$_2$(OTf)$_3$ and Lu(6)$_2$(OTf)$_3$ were synthesized in the same procedure as above.

3. Single Crystal X-ray Diffraction Studies

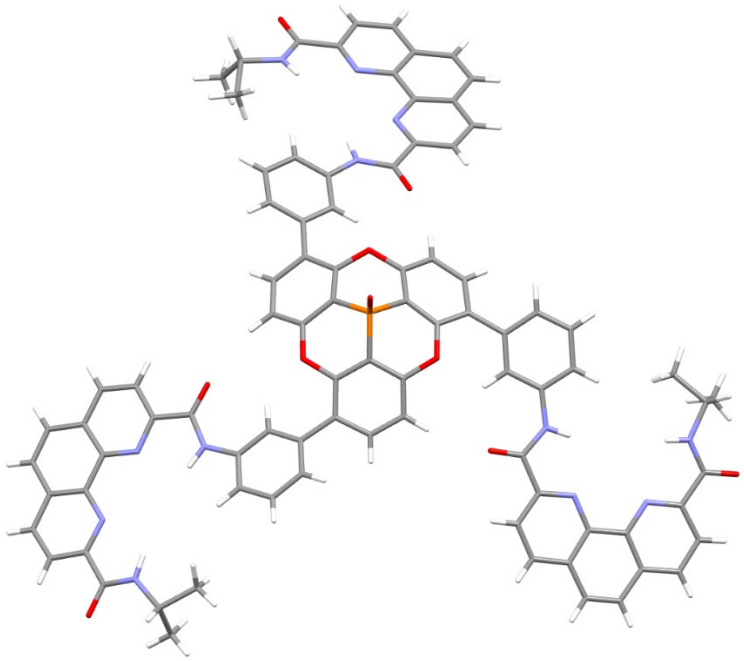

Figure S1. Crystal structure of **L**.

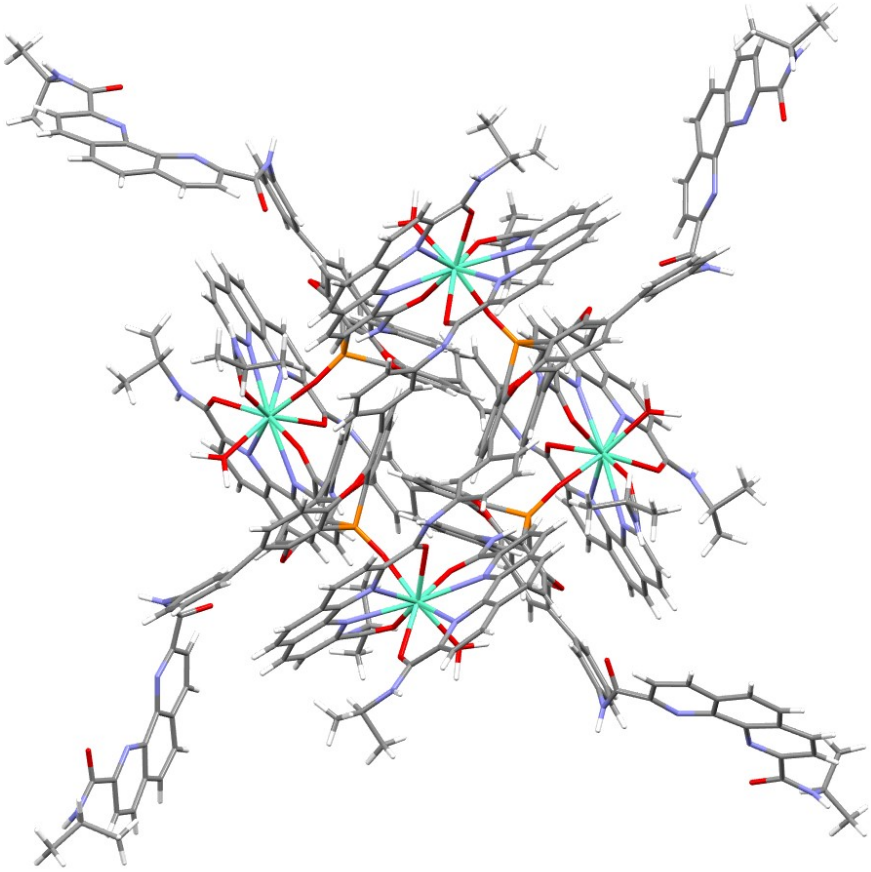

Figure S2. Crystal structure of $\mathbf{Eu_4L_4}$.

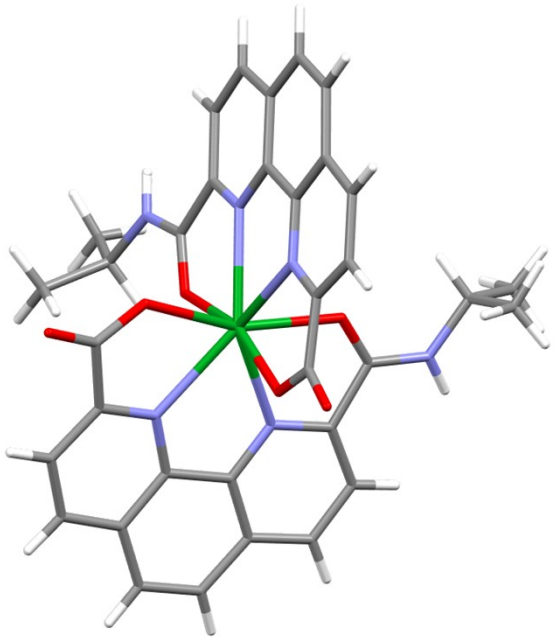

Figure S3. Crystal structure of **Lu(6)$_2$**

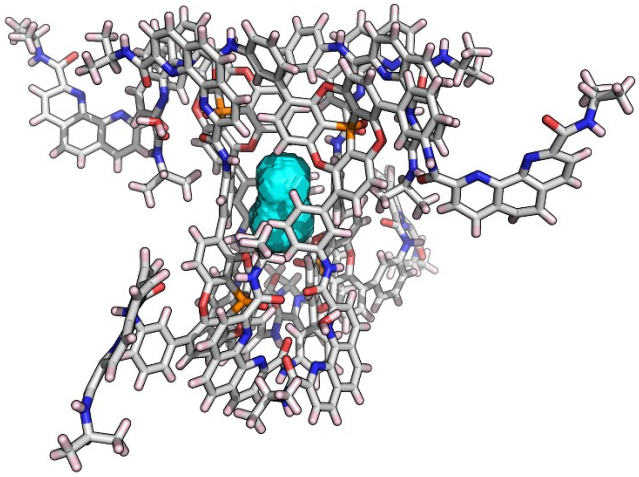

Figure S4. Visualization of the internal cavity volume (50.9 Å^3, cyan surface) within the **Eu$_4$L$_4$** crystal structure, calculated using the MoloVol program. [S4]

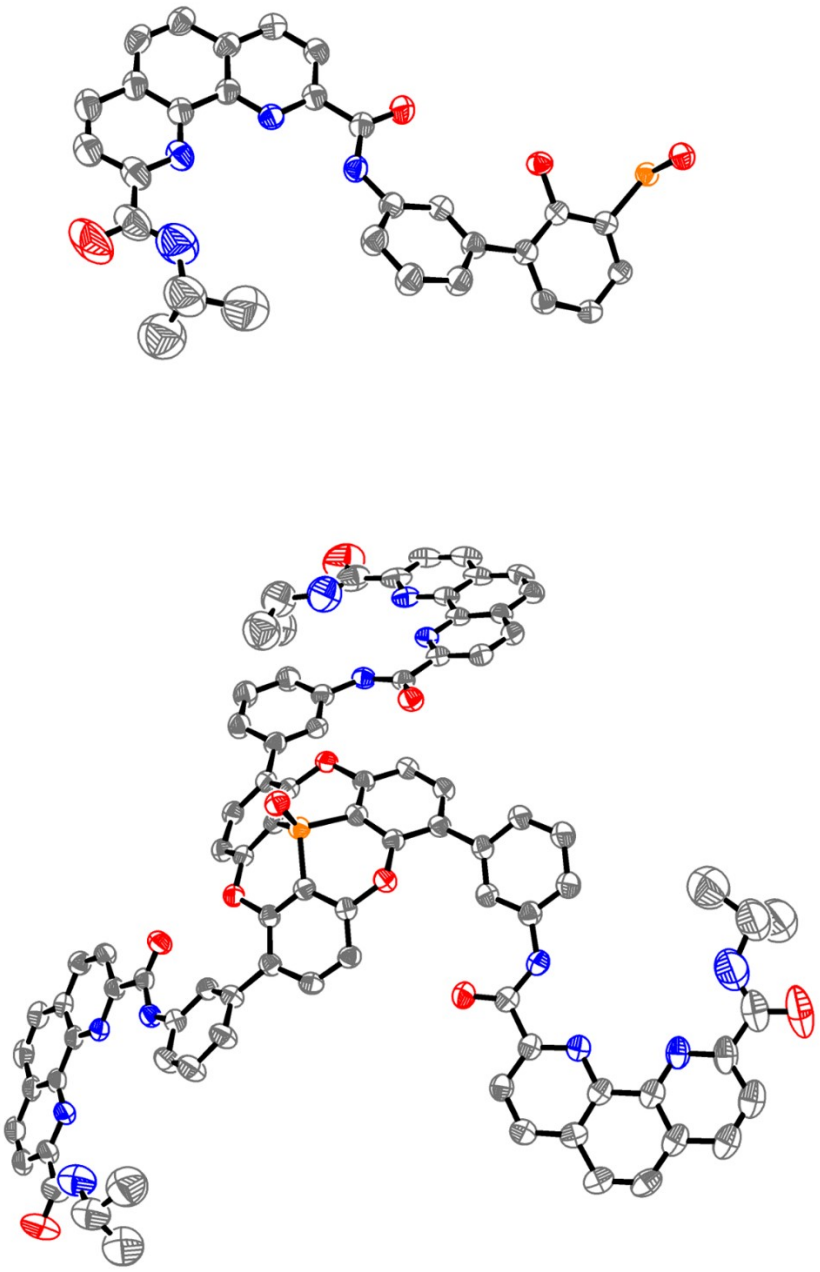

Figure S5. Ortep-3 drawing of the asymmetric unit (up) and the full molecule (down) in the crystal structure of **L** at 30% probability level. [S5]

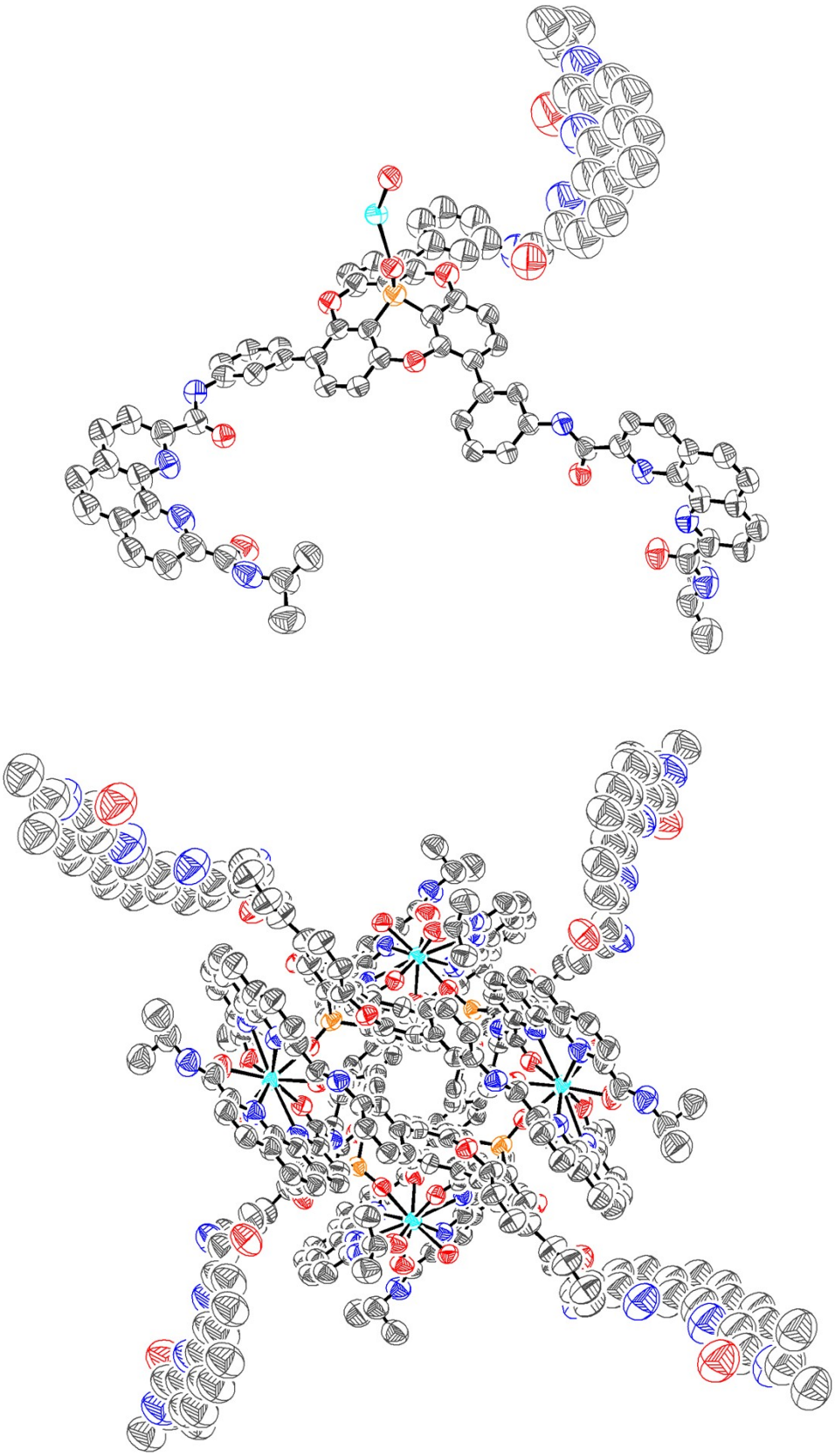

Figure S6. Ortep-3 drawing of the asymmetric unit (up) and the full cage (down) in the crystal structure of $\mathbf{Eu_4L_4}$ at 30% probability level. [S5]

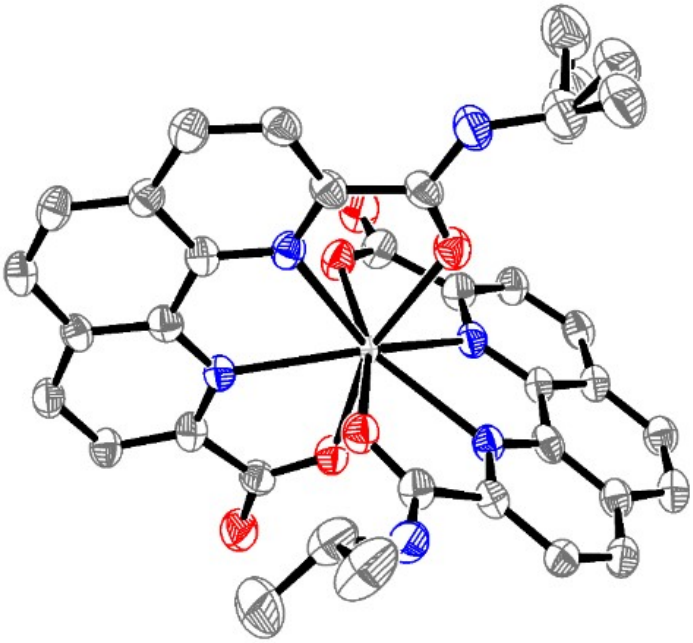

Figure S7. Ortep-3 drawing of the full complex in the crystal structure of **Lu(6)$_2$** at 30% probability level. [S5]

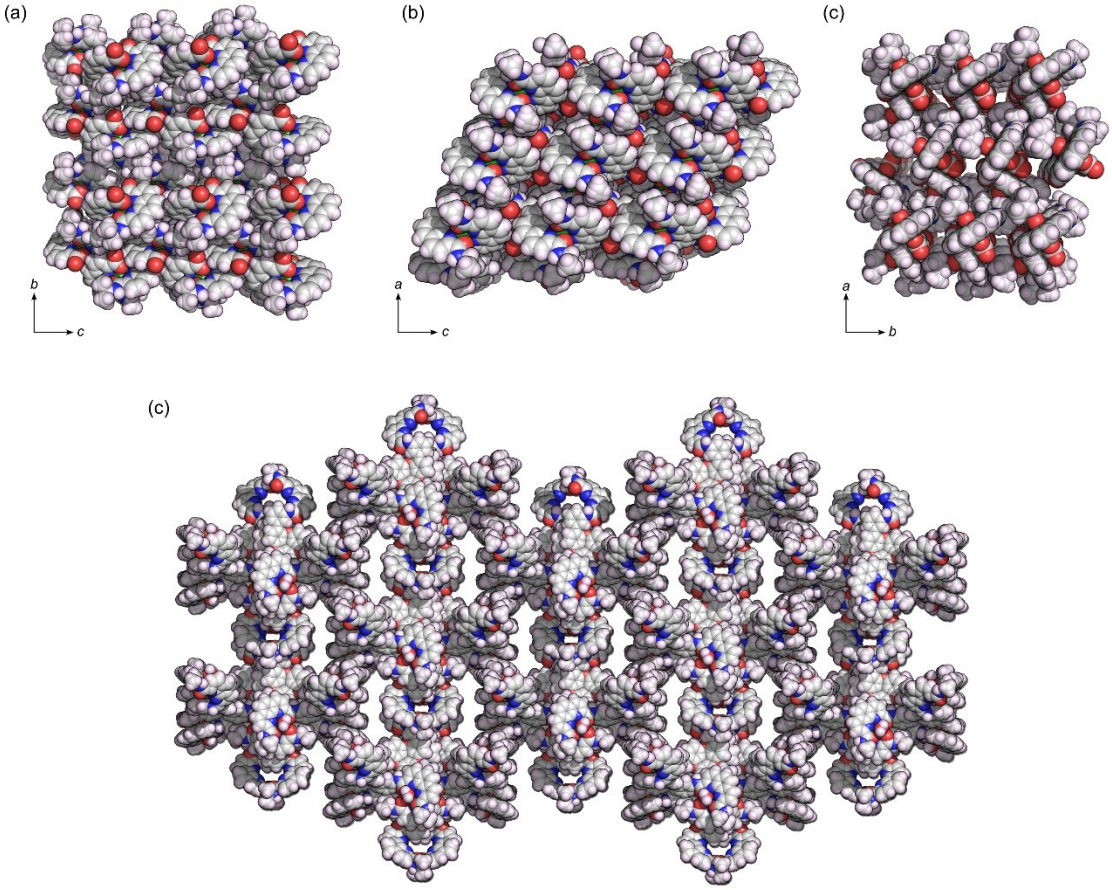

Figure S8. (a-c) Stacking diagrams of the **Lu(6)$_2$** crystal viewed along the *a*-, *b*-, and *c*-axes, respectively. (d) Stacking diagram of the **Eu$_4$L$_4$** crystal viewed along the *a*- or *b*-axis.

Eu_4L_4 exhibited secondary channels along the *a* and *b* axes, facilitating interactions with aldehyde gas molecules, whereas the mononuclear **$Lu(6)_2$** complex featured a closely packed structure that hindered such interactions (Figure R15). PLATON calculations confirmed that **Eu_4L_4** has significantly higher porosity (57.9%) compared to **$Lu(6)_2$** (33.6%), enabling better aldehyde access to the complex.

Table S1. Crystal data and structure refinement for **L**. (CCDC- 2389302)

Identification code	**L**
Empirical formula	$C_{87}H_{60}N_{12}O_{10}P$
Formula weight	1464.44
Temperature/K	150
Crystal system	trigonal
Space group	*P*3*c*1
a/Å	27.6432(9)
b/Å	27.6432(9)
c/Å	15.0008(6)
α/°	90
β/°	90
γ/°	120
Volume/Å^3	9927.1(7)
Z	4
ρ_{calc}g/cm^3	1.248
μ/mm^{-1}	0.879
F(000)	3945.0
Crystal size/mm^3	0.53 × 0.36 × 0.22
Radiation	Cu Kα (λ = 1.54184)
2Θ range for data collection/°	3.69 to 133.196
Index ranges	-30 ≤ h ≤ 32, -25 ≤ k ≤ 32, -17 ≤ l ≤ 15
Reflections collected	33955
Independent reflections	5839 [R_{int} = 0.1231, R_{sigma} = 0.0655]
Data/restraints/parameters	5839/644/331
Goodness-of-fit on F^2	1.435
Final R indexes [I>=2σ (I)]	R_1 = 0.1270, wR_2 = 0.3731
Final R indexes [all data]	R_1 = 0.1488, wR_2 = 0.3955
Largest diff. peak/hole / e Å^{-3}	0.79/-0.59

Table S2. Crystal data and structure refinement for **Eu_4L_4**. (CCDC- 2389303)

Identification code	**Eu_4L_4**
Empirical formula	$C_{348}H_{260}Eu_4N_{48}O_{44}P_4$
Formula weight	6549.74
Temperature/K	100(2)
Crystal system	tetragonal
Space group	$I4_1/a$
a/Å	30.1287(5)
b/Å	30.1287(5)
c/Å	64.0464(16)
α/°	90
β/°	90
γ/°	90
Volume/Å^3	58137(2)
Z	4
ρ_{calc}g/cm^3	0.748
μ/mm^{-1}	2.514
F(000)	13392.0
Crystal size/mm^3	0.35 × 0.21 × 0.2
Radiation	Ga Kα (λ = 1.3405)
2Θ range for data collection/°	4.332 to 67.904
Index ranges	-21≤ h ≤ 19, -25 ≤ k ≤ 19, -40 ≤ l ≤53
Reflections collected	30314
Independent reflections	8638 [R_{int} = 0.0717, R_{sigma} = 0.0652]
Data/restraints/parameters	8638/2686/916
Goodness-of-fit on F^2	1.249
Final R indexes [I>=2σ (I)]	R_1 = 0.1135, wR_2 = 0.2998
Final R indexes [all data]	R_1 = 0.1445, wR_2 = 0.3246
Largest diff. peak/hole / e Å^{-3}	0.96/-0.46

Table S3. Crystal data and structure refinement for **Lu(6)$_2$**. (CCDC- 2389298)

Identification code	**Lu(6)$_2$**
Empirical formula	$C_{34}H_{28}LuN_6O_6$
Formula weight	791.59
Temperature/K	101(2)
Crystal system	monoclinic
Space group	$P2_1/n$
a/Å	11.9192(4)
b/Å	25.0115(5)
c/Å	15.2944(5)
α/°	90
β/°	112.505(4)
γ/°	90
Volume/Å^3	4212.3(2)
Z	4
ρ_{calc}g/cm^3	1.248
μ/mm^{-1}	3.183
F(000)	1572.0
Crystal size/mm^3	0.53 × 0.33 × 0.25
Radiation	micro-focus metaljet (λ = 1.3405)
2Θ range for data collection/°	6.144 to 105.854
Index ranges	$-14 \leq h \leq 12$, $-28 \leq k \leq 29$, $-18 \leq l \leq 18$
Reflections collected	15520
Independent reflections	6966 [R_{int} = 0.0294, R_{sigma} = 0.0362]
Data/restraints/parameters	6966/66/436
Goodness-of-fit on F^2	1.054
Final R indexes [I>=2σ (I)]	R_1 = 0.0654, wR_2 = 0.1985
Final R indexes [all data]	R_1 = 0.0746, wR_2 = 0.2043
Largest diff. peak/hole / e Å^{-3}	1.70/-0.74

4. ESI-TOF-MS Spectra

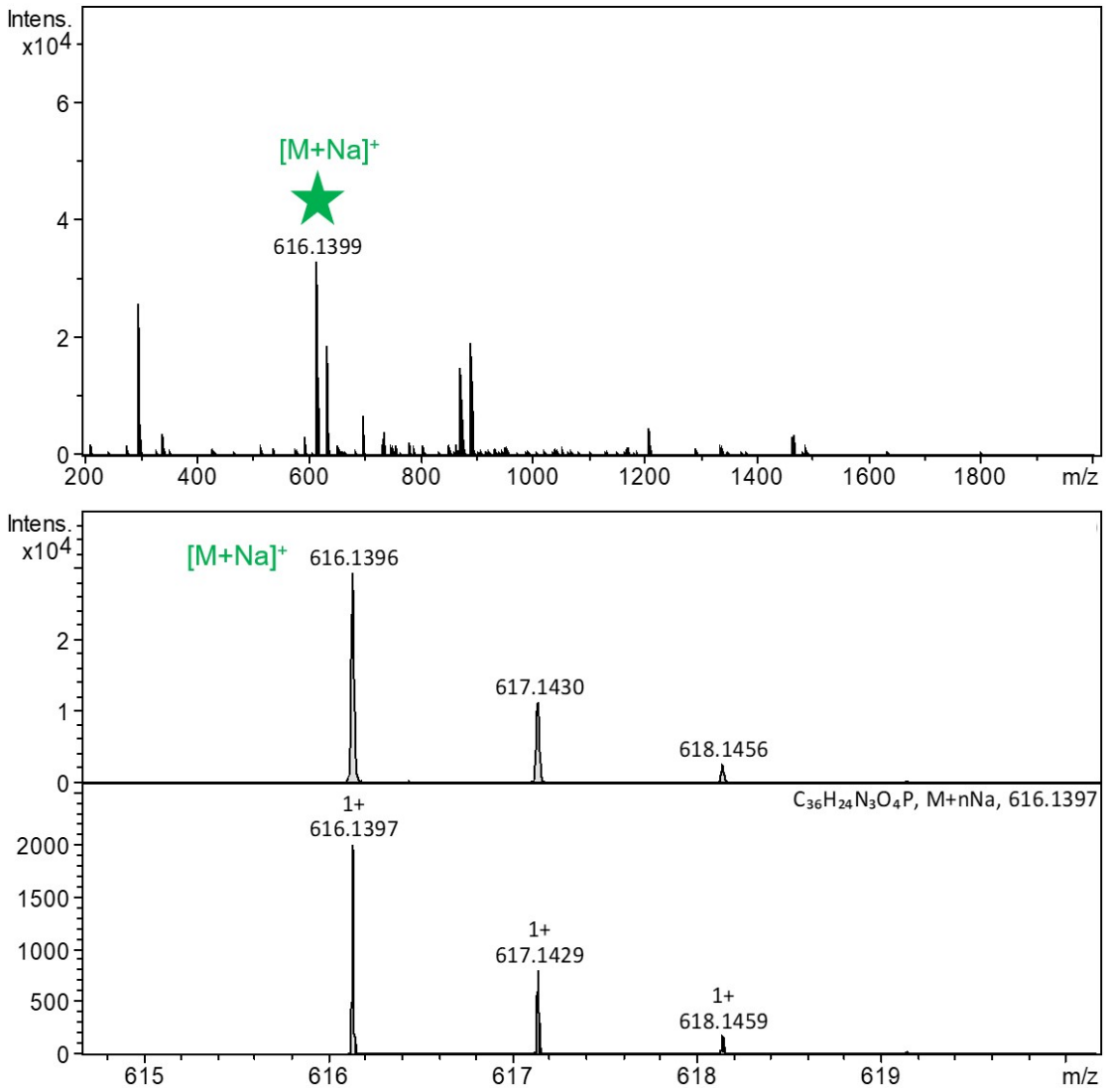

Figure S9. ESI-TOF-MS spectra of **15** in $CHCl_3$.

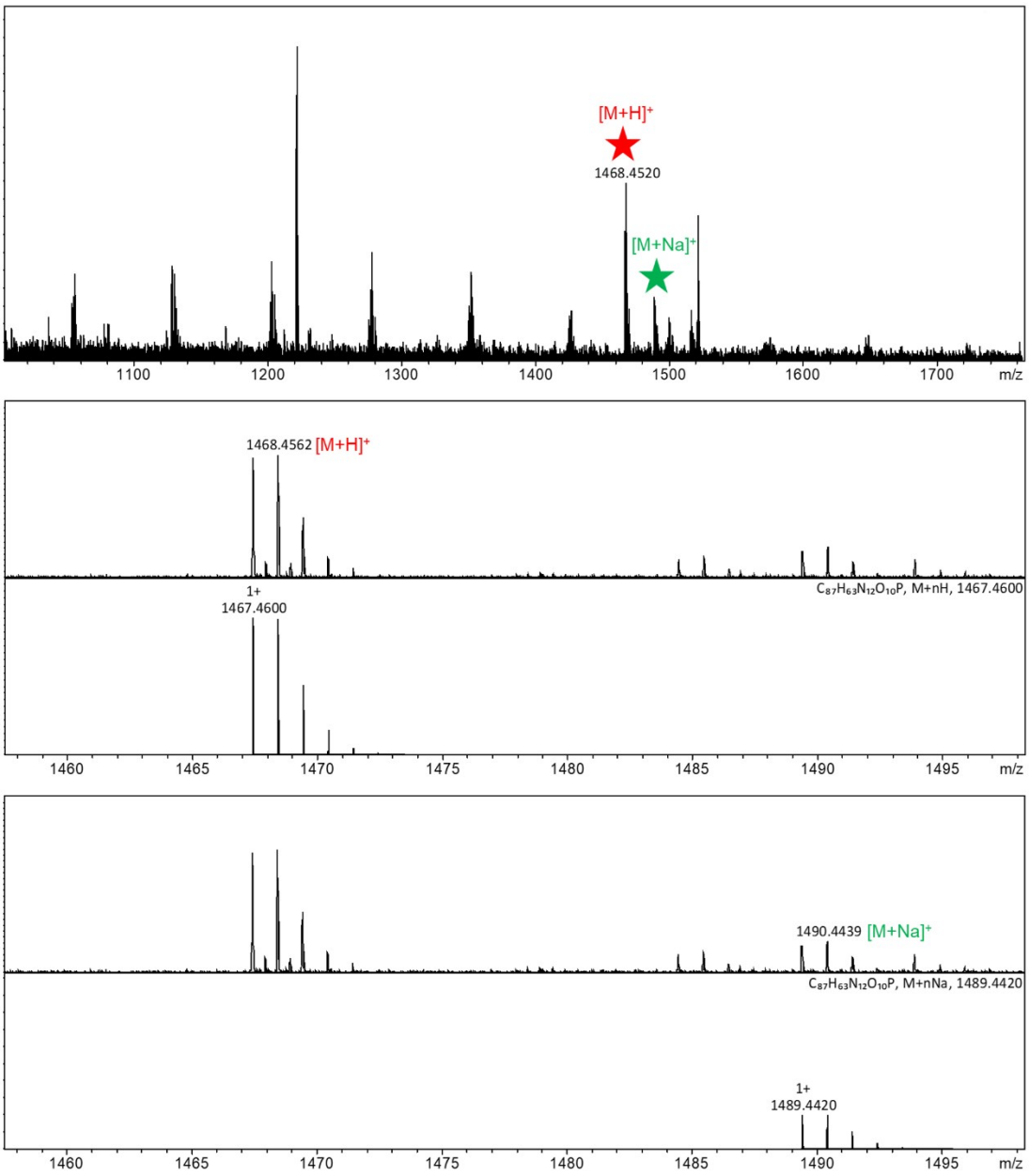

Figure S10. ESI-TOF-MS spectra of **L** in $CHCl_3$.

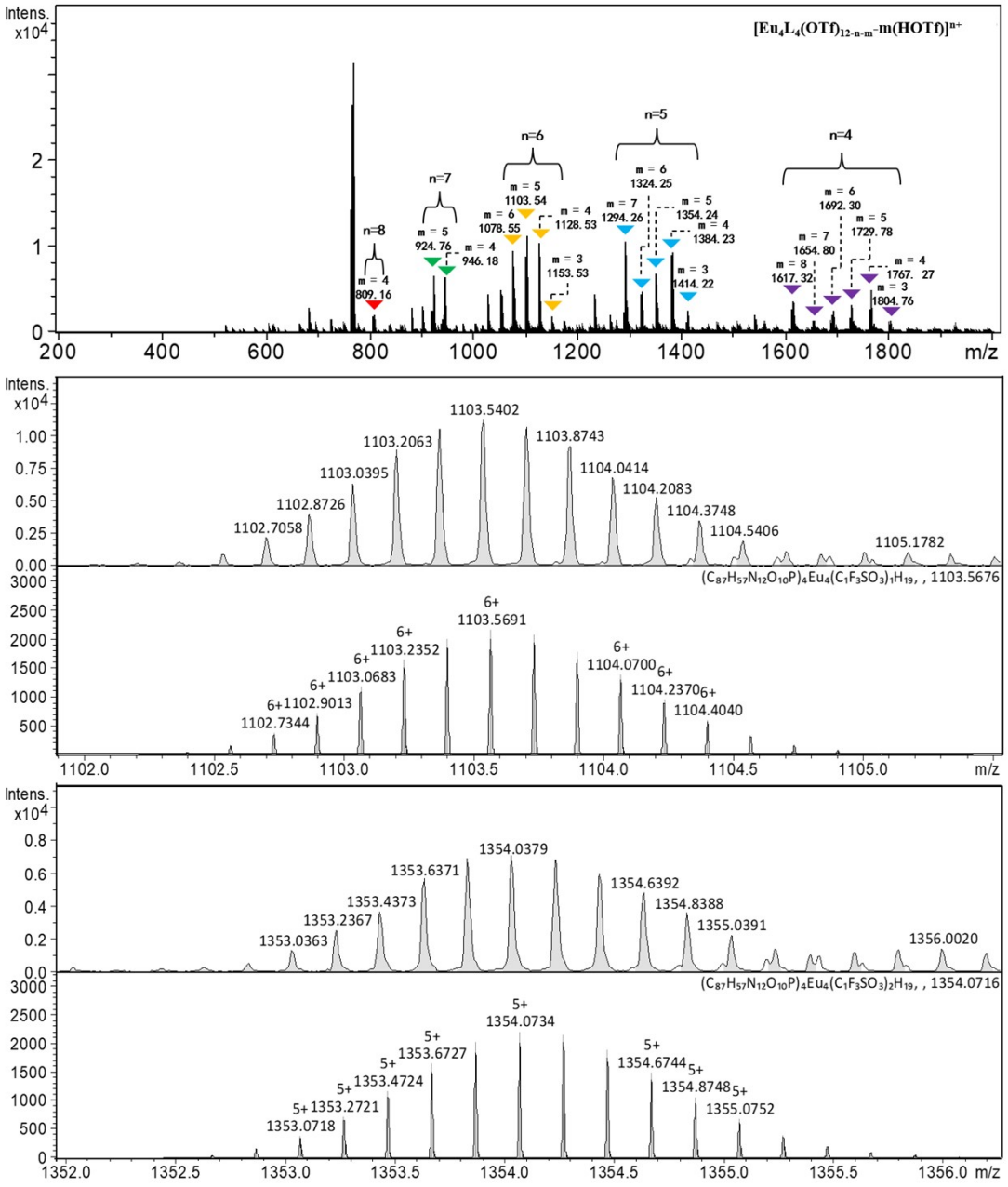

Figure S11 ESI-TOF-MS spectra of **$Eu_4L_4(OTf)_{12}$** in a CH_3CN/CH_3OH (v/v = 2/1) mixture. The trifluoromethanesulfonate ($CF_3SO_3^-$) anions and protons on amide groups are easily lost, resulting in various isotopic patterns.

Table S4. Comparison of the observed and simulated signals in the ESI-MS spectrum of **$Eu_4L_4(OTf)_{12}$** in a CH_3CN/CH_3OH (v/v = 2/1) mixture.

Valence	Molecular Formula	Observed	Simulated
+8	$[Eu_4(C_{87}H_{63}N_{12}O_{10}P)_4(OTf)_0\text{-}4(HOTf)]^{8+}$	809.16	809.18
+7	$[Eu_4(C_{87}H_{63}N_{12}O_{10}P)_4(OTf)_0\text{-}5(HOTf)]^{7+}$	924.76	924.78
	$[Eu_4(C_{87}H_{63}N_{12}O_{10}P)_4(OTf)_1\text{-}4(HOTf)]^{7+}$	946.18	946.20
+6	$[Eu_4(C_{87}H_{63}N_{12}O_{10}P)_4(OTf)_0\text{-}6(HOTf)]^{6+}$	1078.55	1078.58
	$[Eu_4(C_{87}H_{63}N_{12}O_{10}P)_4(OTf)_1\text{-}5(HOTf)]^{6+}$	1103.54	1103.57
	$[Eu_4(C_{87}H_{63}N_{12}O_{10}P)_4(OTf)_2\text{-}4(HOTf)]^{6+}$	1128.53	1128.56
	$[Eu_4(C_{87}H_{63}N_{12}O_{10}P)_4(OTf)_3\text{-}3(HOTf)]^{6+}$	1153.53	1153.56
+5	$[Eu_4(C_{87}H_{63}N_{12}O_{10}P)_4(OTf)_0\text{-}7(HOTf)]^{5+}$	1294.26	1294.29
	$[Eu_4(C_{87}H_{63}N_{12}O_{10}P)_4(OTf)_1\text{-}6(HOTf)]^{5+}$	1324.25	1324.28
	$[Eu_4(C_{87}H_{63}N_{12}O_{10}P)_4(OTf)_2\text{-}5(HOTf)]^{5+}$	1354.24	1354.27
	$[Eu_4(C_{87}H_{63}N_{12}O_{10}P)_4(OTf)_3\text{-}4(HOTf)]^{5+}$	1384.23	1324.27
	$[Eu_4(C_{87}H_{63}N_{12}O_{10}P)_4(OTf)_4\text{-}3(HOTf)]^{5+}$	1414.22	1414.26
+4	$[Eu_4(C_{87}H_{63}N_{12}O_{10}P)_4(OTf)_0\text{-}8(HOTf)]^{4+}$	1617.32	1617.36
	$[Eu_4(C_{87}H_{63}N_{12}O_{10}P)_4(OTf)_1\text{-}7(HOTf)]^{4+}$	1654.80	1654.85
	$[Eu_4(C_{87}H_{63}N_{12}O_{10}P)_4(OTf)_2\text{-}6(HOTf)]^{4+}$	1692.30	1692.34
	$[Eu_4(C_{87}H_{63}N_{12}O_{10}P)_4(OTf)_3\text{-}5(HOTf)]^{4+}$	1729.78	1729.83
	$[Eu_4(C_{87}H_{63}N_{12}O_{10}P)_4(OTf)_4\text{-}4(HOTf)]^{4+}$	1767.27	1767.32
	$[Eu_4(C_{87}H_{63}N_{12}O_{10}P)_4(OTf)_5\text{-}3(HOTf)]^{4+}$	1804.76	1804.81

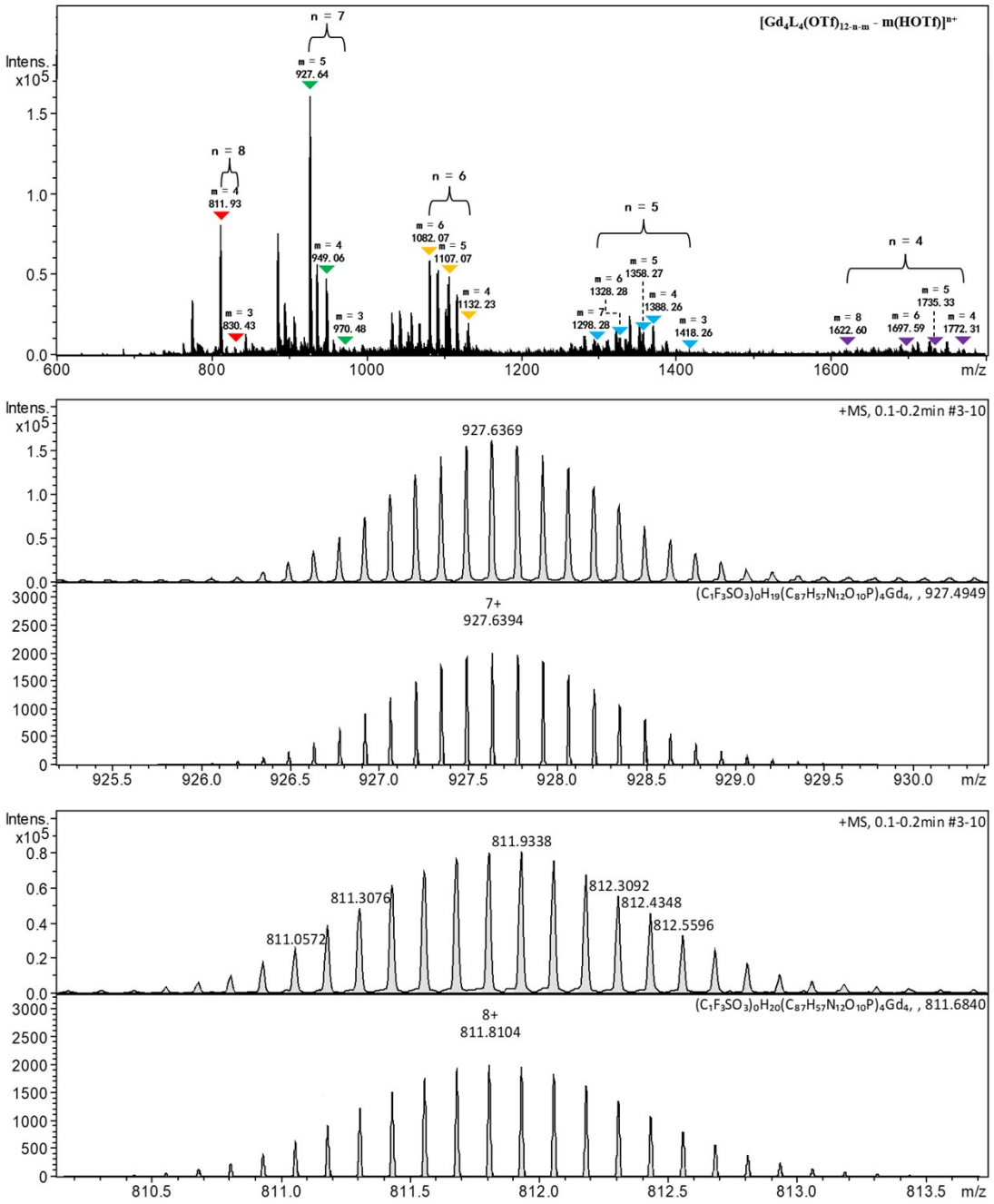

Figure S12. ESI-TOF-MS spectra of **$Gd_4L_4(OTf)_{12}$** in a CH_3CN/CH_3OH (v/v = 2/1) mixture. The trifluoromethanesulfonate ($CF_3SO_3^-$) anions and protons on the amide groups are readily lost, resulting in various isotopic patterns.

Table S5. Comparison of the observed and simulated signals in the ESI-MS spectrum of **$Gd_4L_4(OTf)_{12}$** in a CH_3CN/CH_3OH (v/v = 2/1) mixture.

Valence	Molecular Formula	Observed	Simulated
+8	$[Gd_4(C_{87}H_{63}N_{12}O_{10}P)_4(OTf)_0\text{-}4(HOTf)]^{8+}$	811.93	811.94
	$[Gd_4(C_{87}H_{63}N_{12}O_{10}P)_4(OTf)_1\text{-}3(HOTf)]^{8+}$	830.43	830.43
+7	$[Gd_4(C_{87}H_{63}N_{12}O_{10}P)_4(OTf)_0\text{-}5(HOTf)]^{7+}$	927.64	927.64
	$[Gd_4(C_{87}H_{63}N_{12}O_{10}P)_4(OTf)_1\text{-}4(HOTf)]^{7+}$	949.06	949.06
	$[Gd_4(C_{87}H_{63}N_{12}O_{10}P)_4(OTf)_2\text{-}3(HOTf)]^{7+}$	970.48	970.49
+6	$[Gd_4(C_{87}H_{63}N_{12}O_{10}P)_4(OTf)_0\text{-}6(HOTf)]^{6+}$	1082.07	1082.08
	$[Gd_4(C_{87}H_{63}N_{12}O_{10}P)_4(OTf)_1\text{-}5(HOTf)]^{6+}$	1107.07	1107.07
	$[Gd_4(C_{87}H_{63}N_{12}O_{10}P)_4(OTf)_2\text{-}4(HOTf)]^{6+}$	1132.23	1132.23
+5	$[Gd_4(C_{87}H_{63}N_{12}O_{10}P)_4(OTf)_0\text{-}7(HOTf)]^{5+}$	1298.28	1298.29
	$[Gd_4(C_{87}H_{63}N_{12}O_{10}P)_4(OTf)_1\text{-}6(HOTf)]^{5+}$	1328.28	1328.28
	$[Gd_4(C_{87}H_{63}N_{12}O_{10}P)_4(OTf)_2\text{-}5(HOTf)]^{5+}$	1358.27	1358.28
	$[Gd_4(C_{87}H_{63}N_{12}O_{10}P)_4(OTf)_3\text{-}4(HOTf)]^{5+}$	1388.26	1388.27
	$[Gd_4(C_{87}H_{63}N_{12}O_{10}P)_4(OTf)_4\text{-}3(HOTf)]^{5+}$	1418.26	1418.26
+4	$[Gd_4(C_{87}H_{63}N_{12}O_{10}P)_4(OTf)_0\text{-}8(HOTf)]^{4+}$	1622.60	1622.61
	$[Gd_4(C_{87}H_{63}N_{12}O_{10}P)_4(OTf)_2\text{-}6(HOTf)]^{4+}$	1697.59	1697.59
	$[Gd_4(C_{87}H_{63}N_{12}O_{10}P)_4(OTf)_3\text{-}5(HOTf)]^{4+}$	1735.33	1735.33
	$[Gd_4(C_{87}H_{63}N_{12}O_{10}P)_4(OTf)_4\text{-}4(HOTf)]^{4+}$	1772.31	1772.32

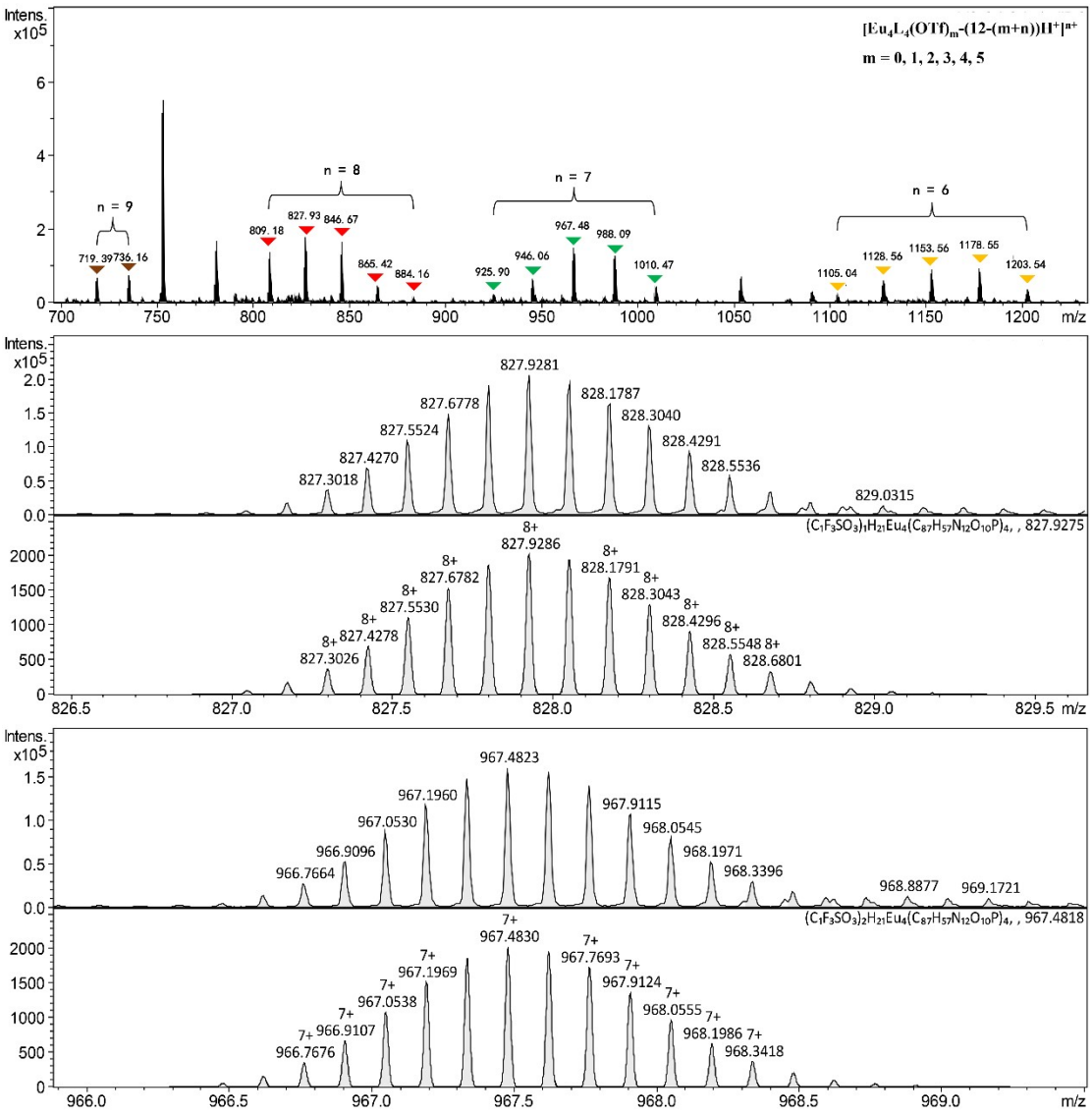

Figure S13. ESI-TOF-MS spectra of **$Eu_4L_4(OTf)_{12}$** in a CH_3CN/CH_3OH/AA (v/v/v = 20/10/3) mixture. The trifluoromethanesulfonate ($CF_3SO_3^-$) anions and protons on amide groups are easily lost, resulting in various isotopic patterns.

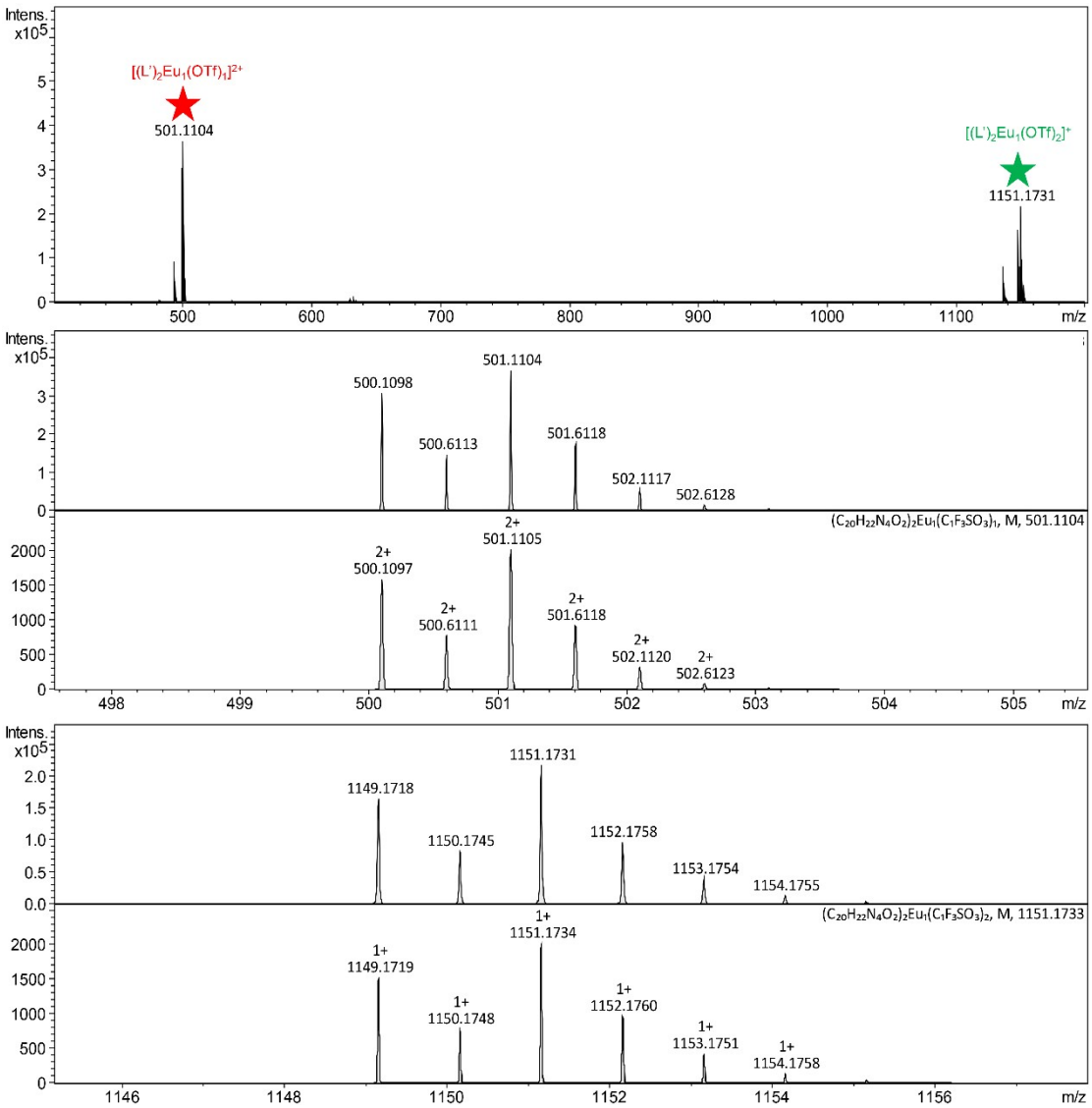

Figure S14. ESI-TOF-MS spectra of **Eu(L')$_2$(OTf)$_3$** in a CH_3CN/CH_3OH (v/v = 2/1) mixture.

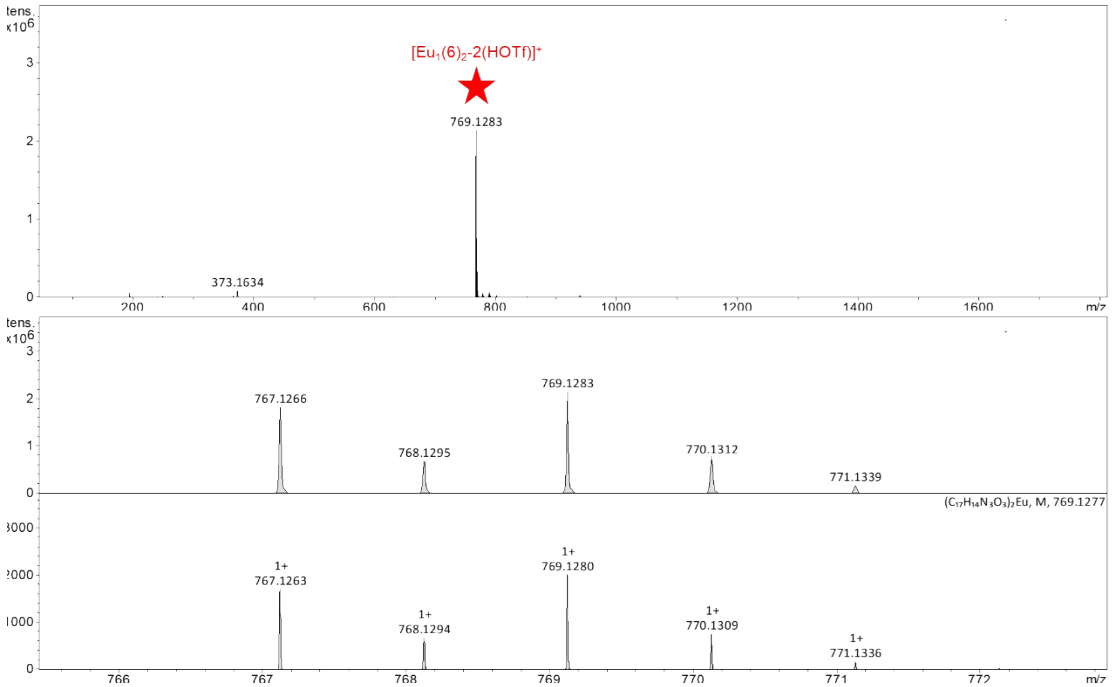

Figure S15. ESI-TOF-MS spectra of **Eu(6)$_2$(OTf)$_3$** in a CH_3CN/CH_3OH (v/v = 2/1) mixture.

5. NMR Spectra

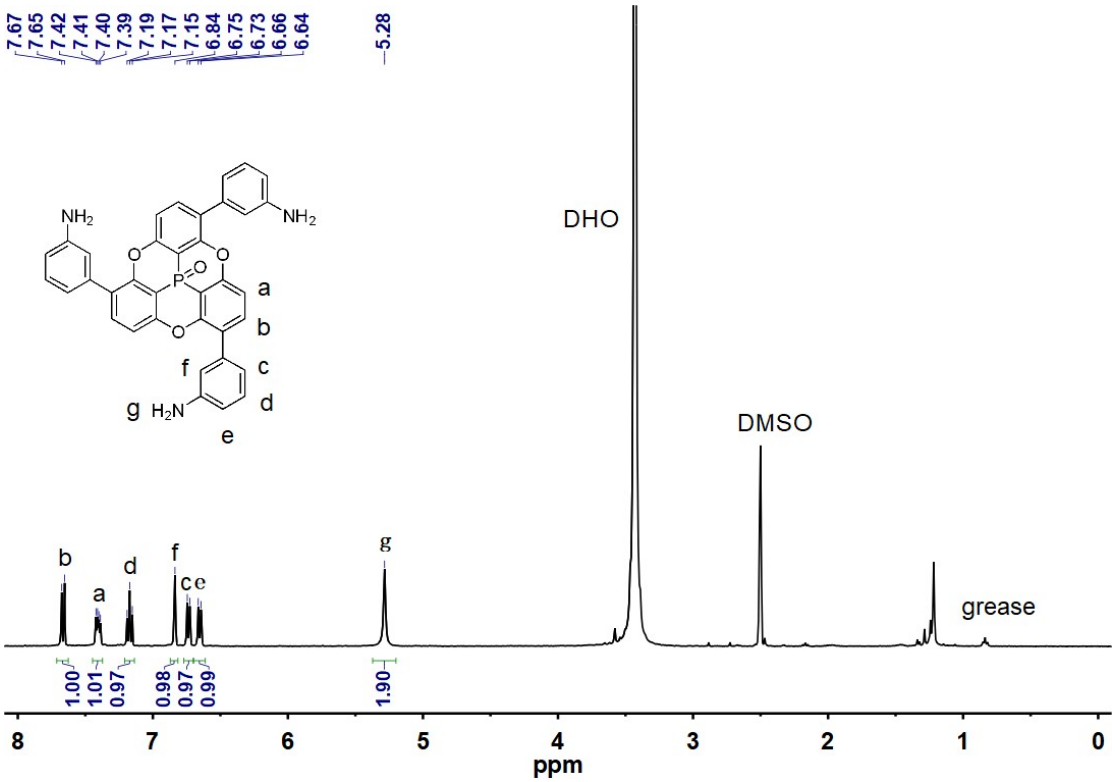

Figure S16. The ^{1}H NMR spectrum of **15** (400 MHz, DMSO-d_6, 298 K).

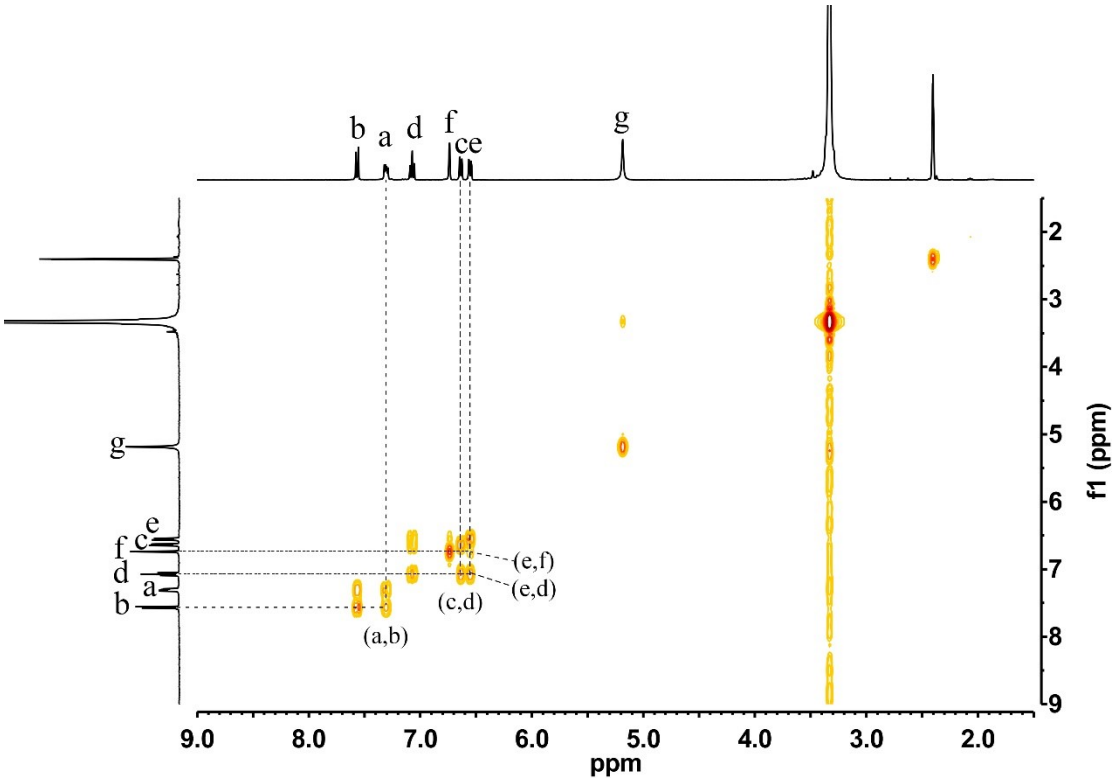

Figure S17. The ^{1}H-^{1}H COSY NMR spectrum of **15** (400 MHz, DMSO-d_6, 298 K).

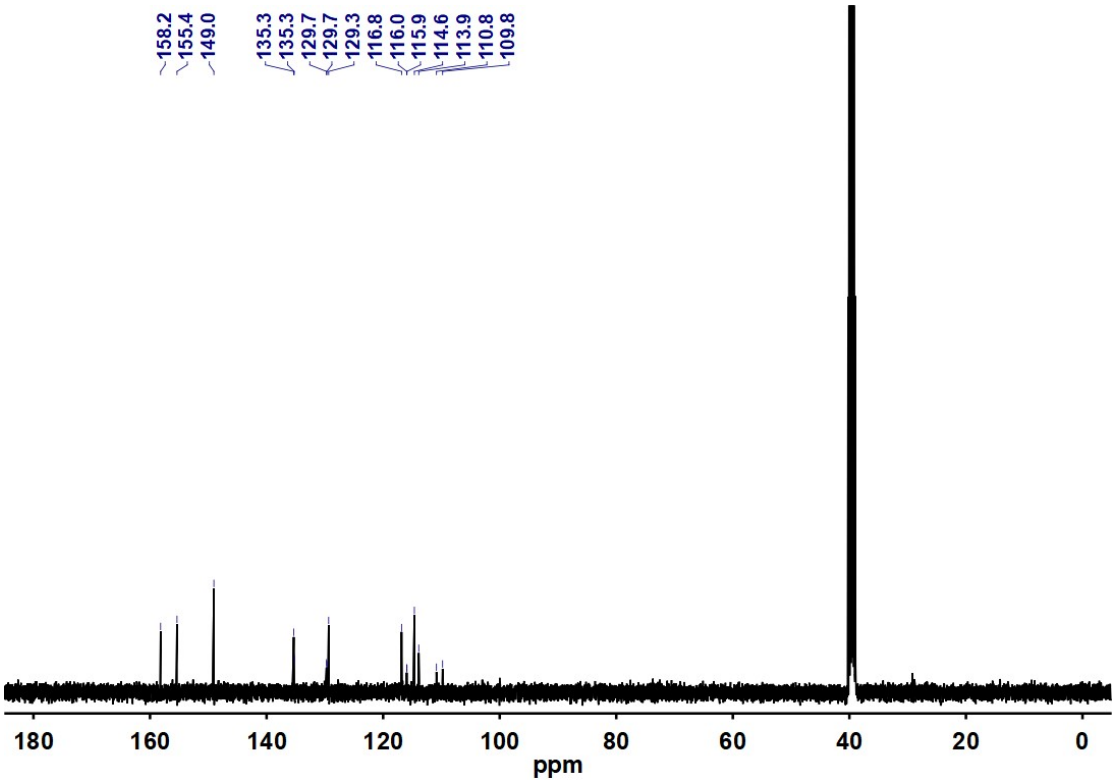

Figure S18. The ^{13}C NMR spectrum of **15** (101 MHz, DMSO-d_6, 298 K).

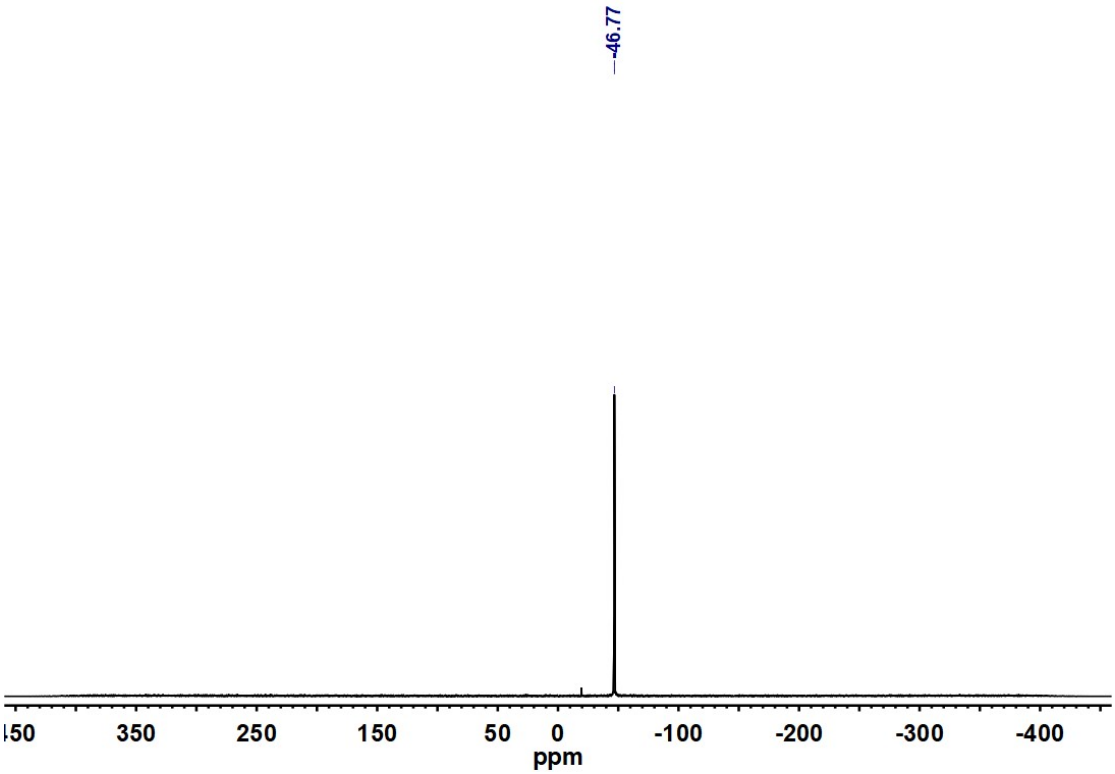

Figure S19. The ^{31}P NMR spectrum of **15** (243 MHz, DMSO-d_6, 298 K).

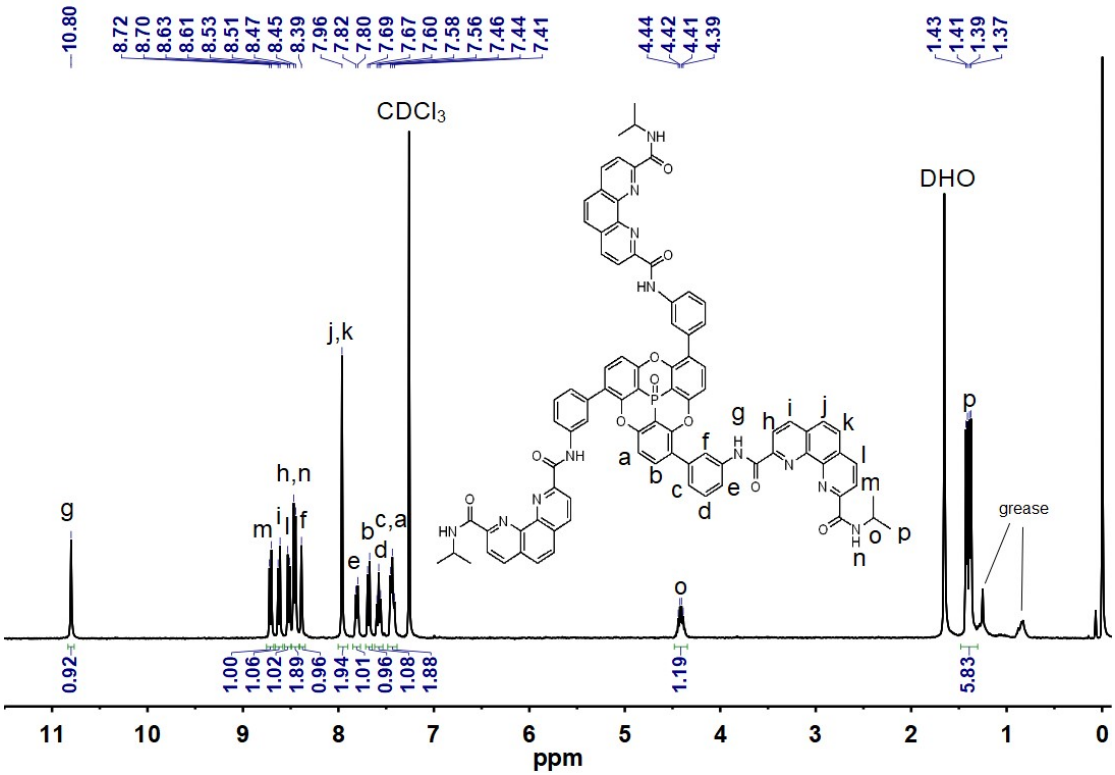

Figure S20. The ^{1}H NMR spectrum of **L** (400 MHz, $CDCl_3$, 298 K).

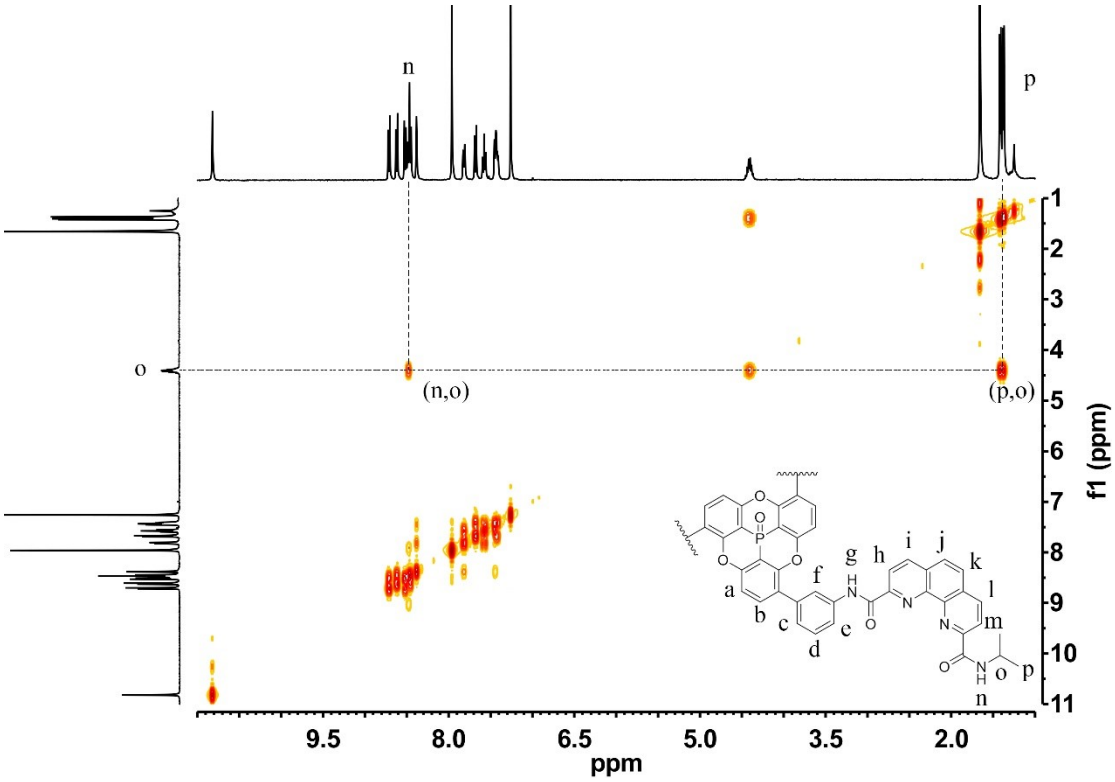

Figure S21. The ^{1}H-^{1}H COSY NMR spectrum of **L** (400 MHz, $CDCl_3$, 298 K).

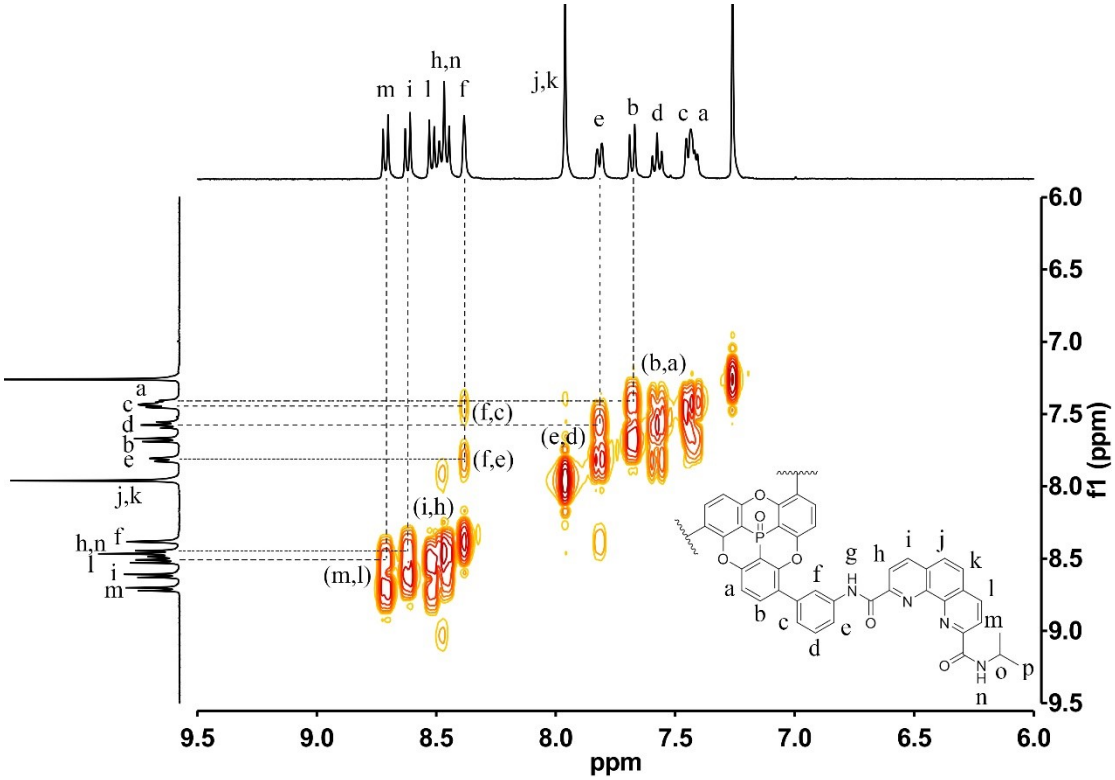

Figure S22. The partial enlargement of ^{1}H-^{1}H COSY NMR spectrum of **L** (400 MHz, $CDCl_3$, 298 K).

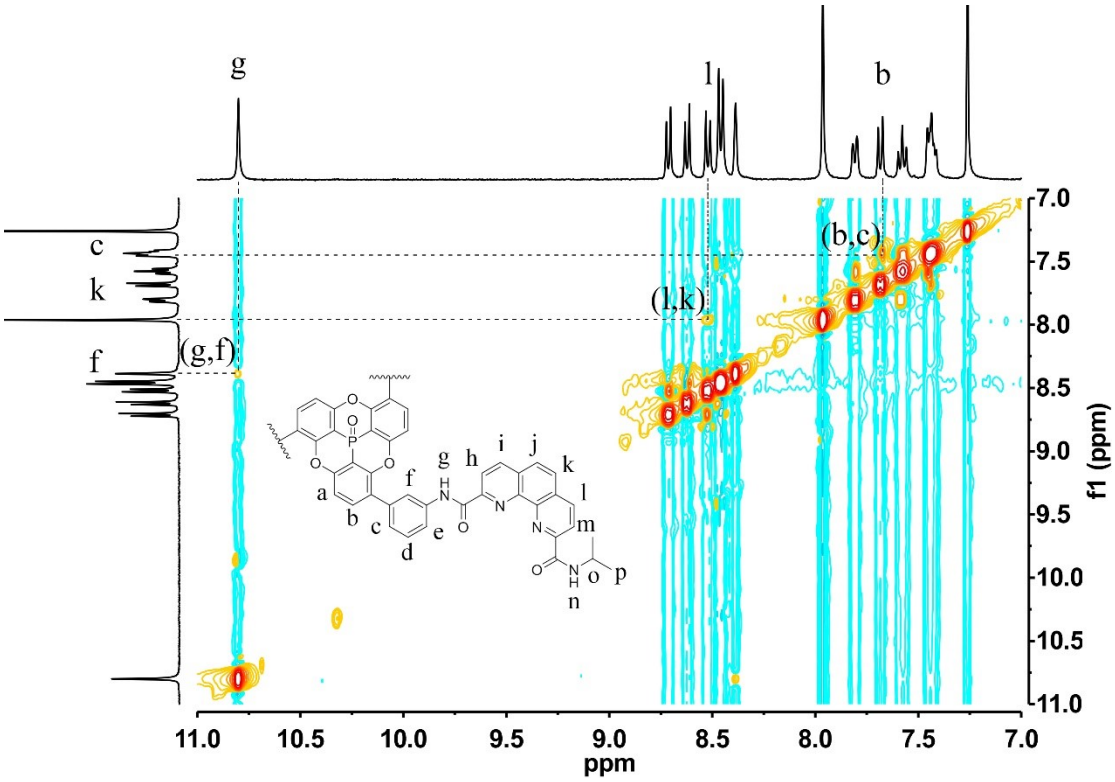

Figure S23. The ^{1}H-^{1}H NOESY NMR spectrum of **L** (400 MHz, $CDCl_3$, 298 K).

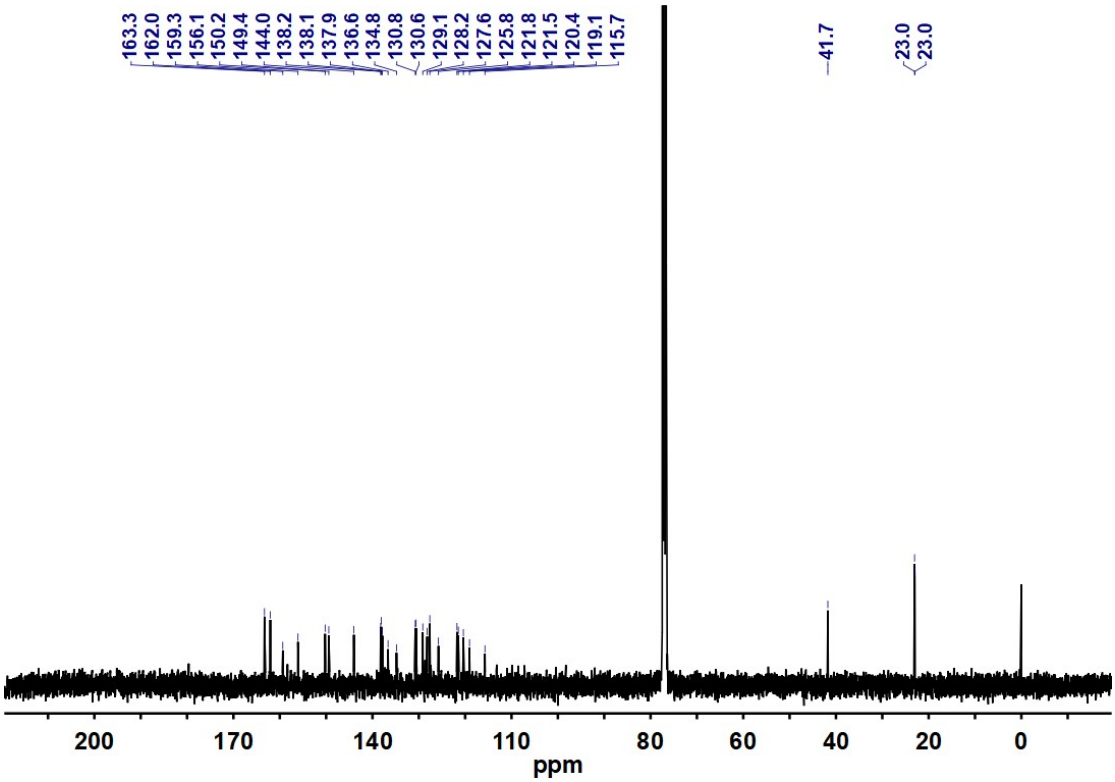

Figure S24. The ^{13}C NMR spectrum of **L** (101 MHz, $CDCl_3$, 298 K).

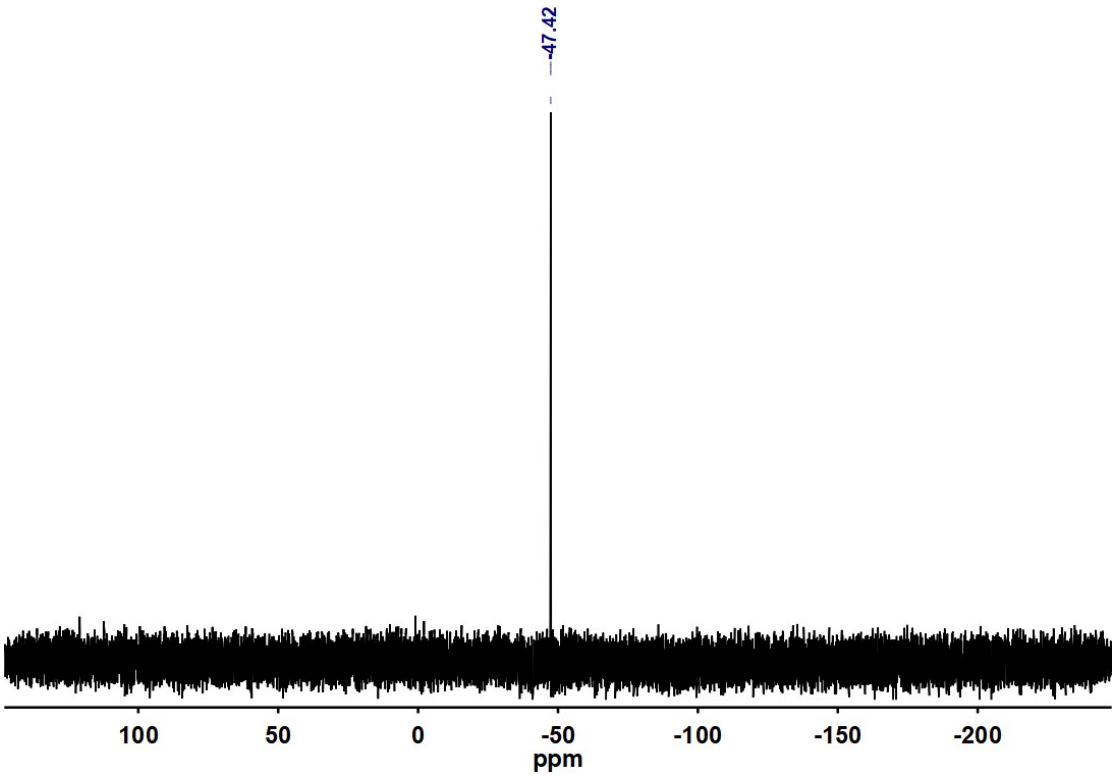

Figure S25. The ^{31}P NMR spectrum of **L** (243 MHz, $CDCl_3$, 298 K).

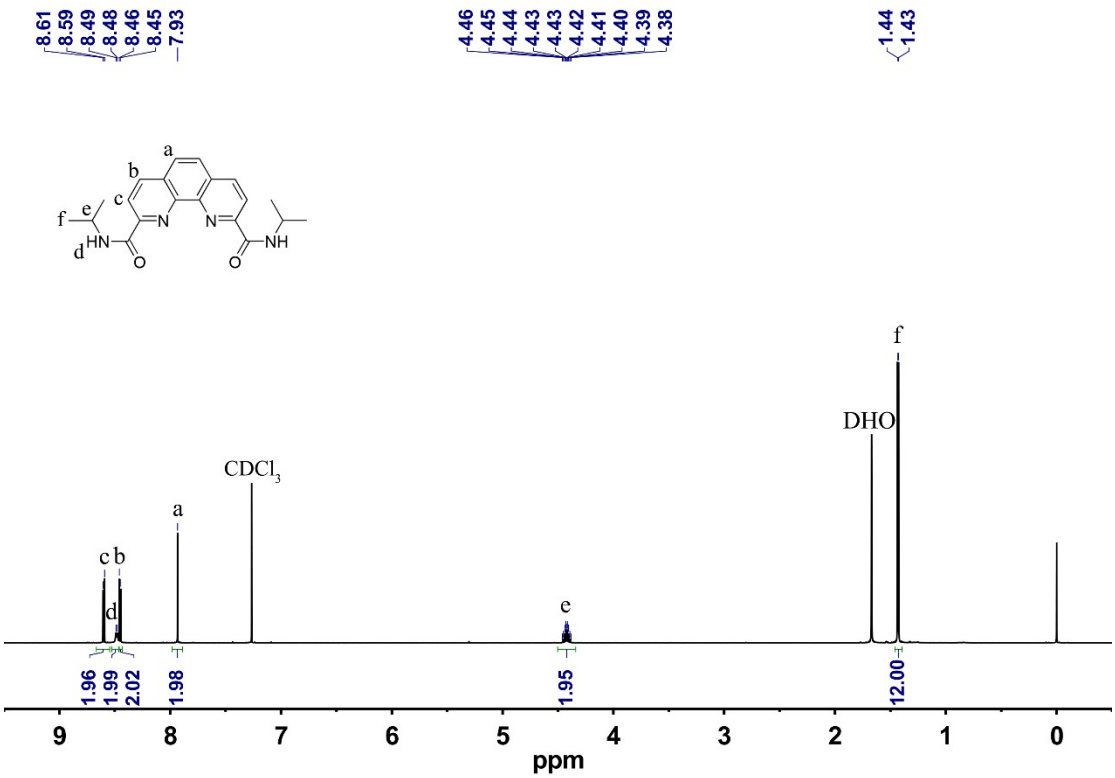

Figure S26. The ^{1}H NMR spectrum of **L'** (600 MHz, $CDCl_3$, 298 K).

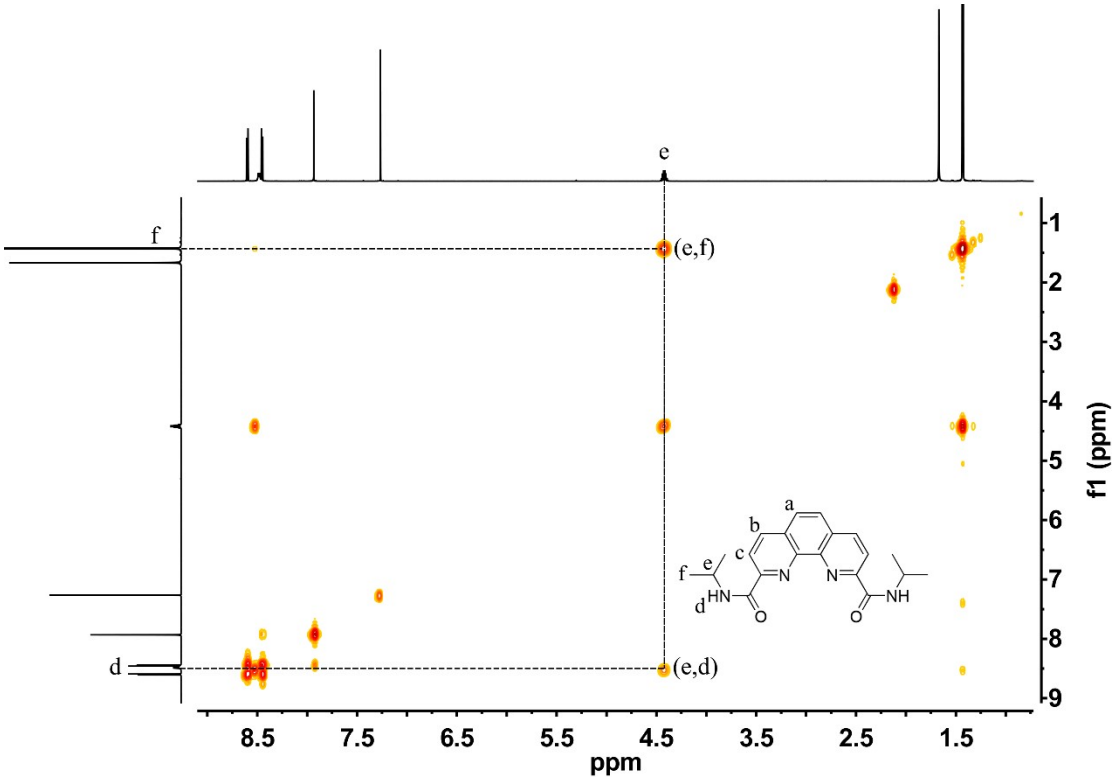

Figure S27. The ^{1}H-^{1}H COSY NMR spectrum of **L'** (400 MHz, $CDCl_3$, 298 K).

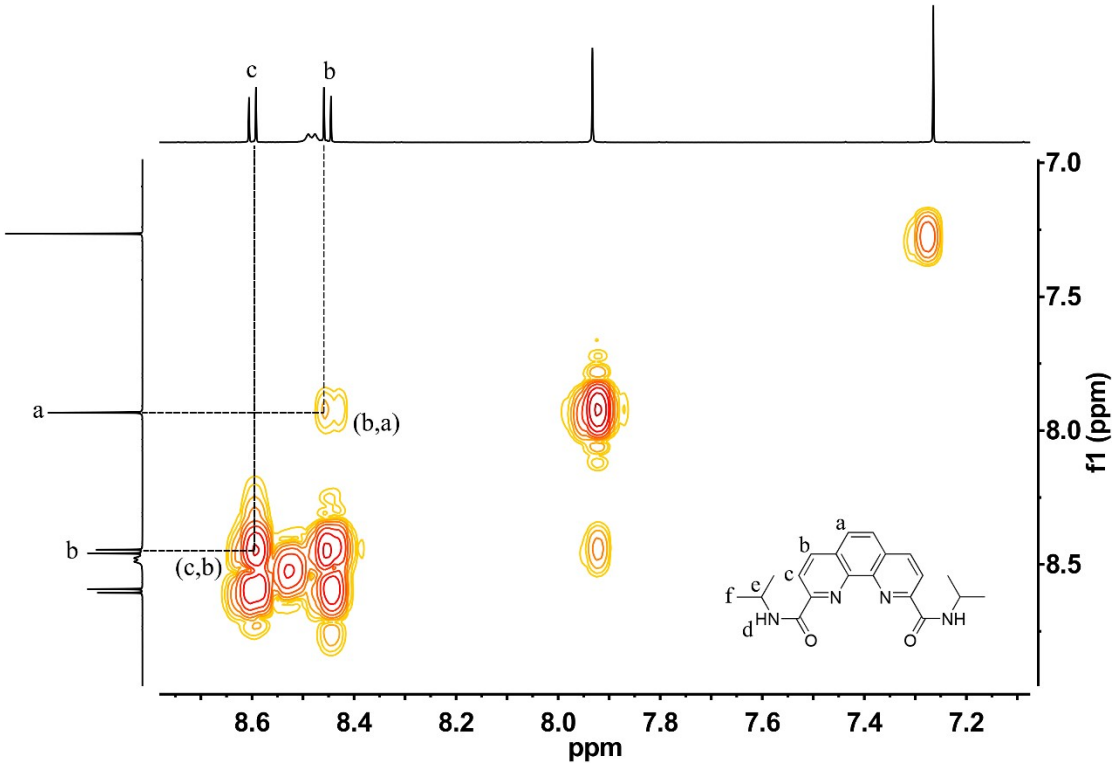

Figure S28. The partial enlargement of ^{1}H-^{1}H COSY NMR spectrum of **L'** (600 MHz, $CDCl_3$, 298 K).

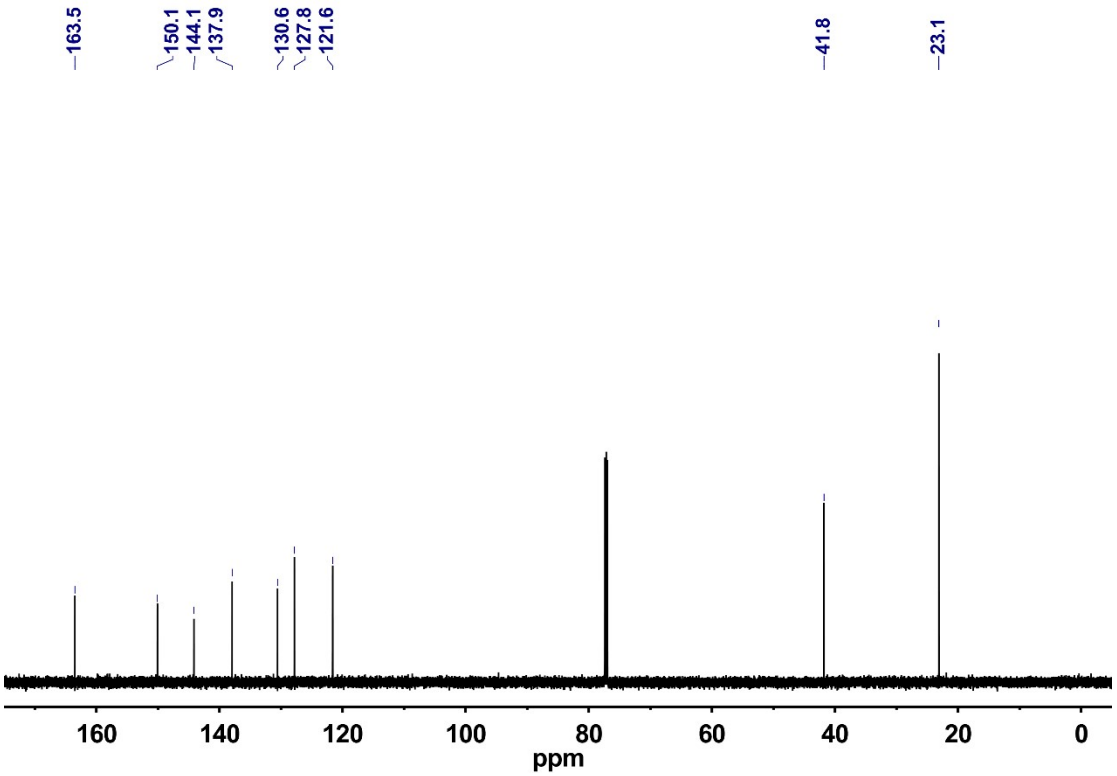

Figure S29. The ^{13}C NMR spectrum of **L'** (151 MHz, $CDCl_3$, 298 K).

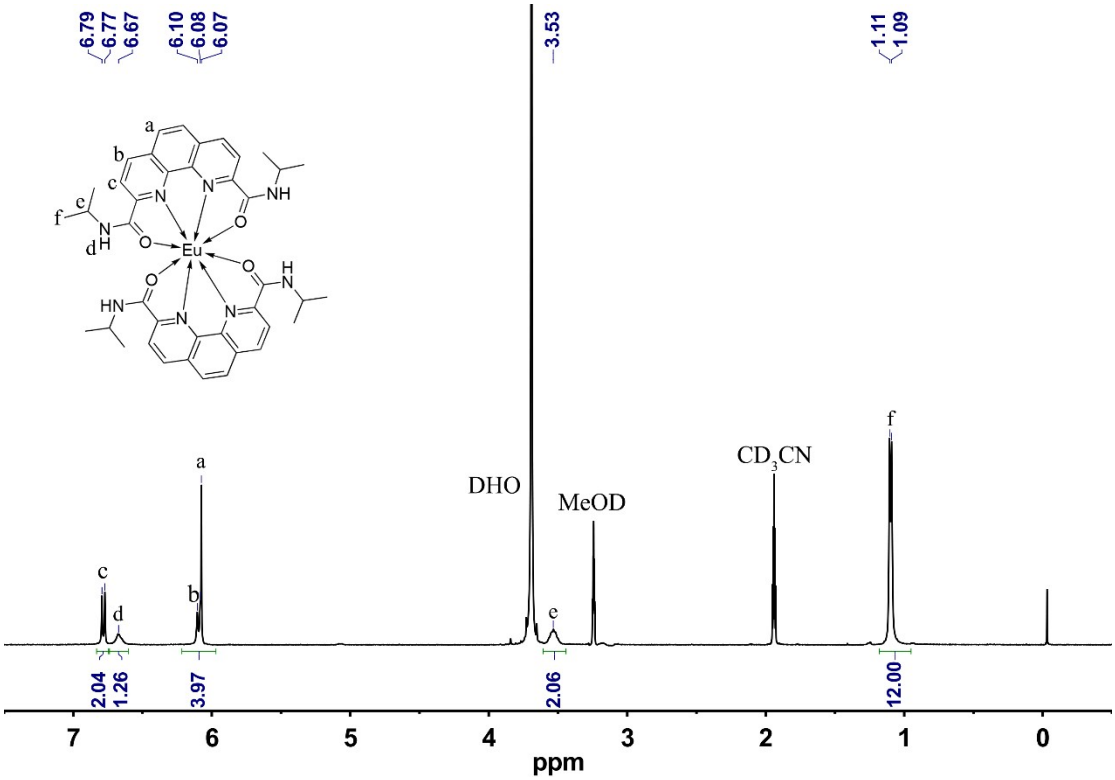

Figure S30. The ^{1}H NMR spectrum of **Eu(L')$_2$** (600 MHz, CD_3CN/CD_3OD v/v = 2/1, 298 K).

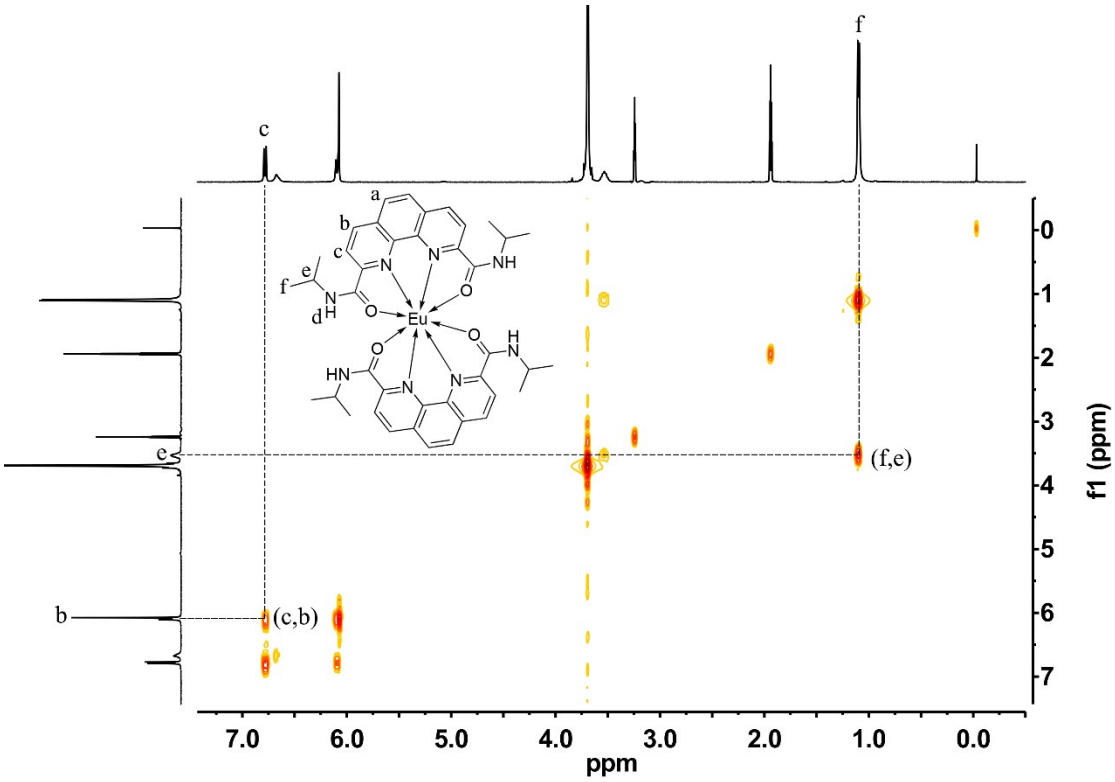

Figure S31. The ^{1}H-^{1}H COSY NMR spectrum of **Eu(L')$_2$** (400 MHz, CD_3CN/CD_3OD v/v = 2/1, 298 K).

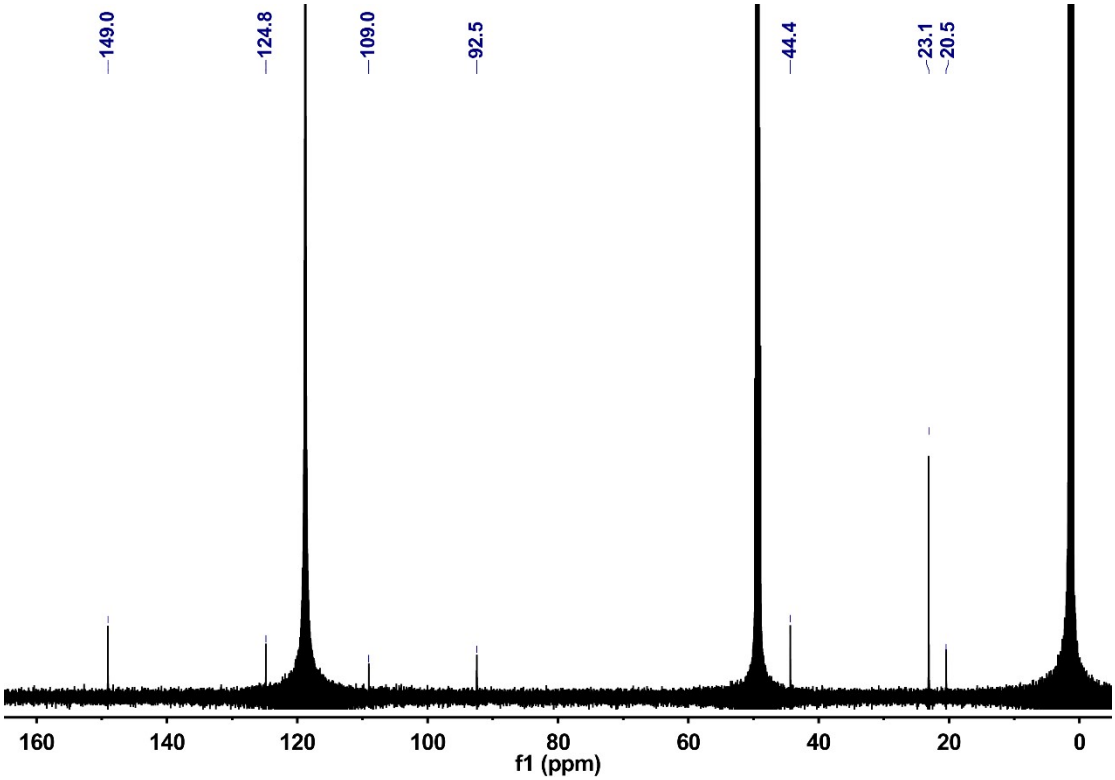

Figure S32. The ^{13}C NMR spectrum of **Eu(L')$_2$** (151 MHz, CD_3CN/CD_3OD v/v = 2/1, 298 K).

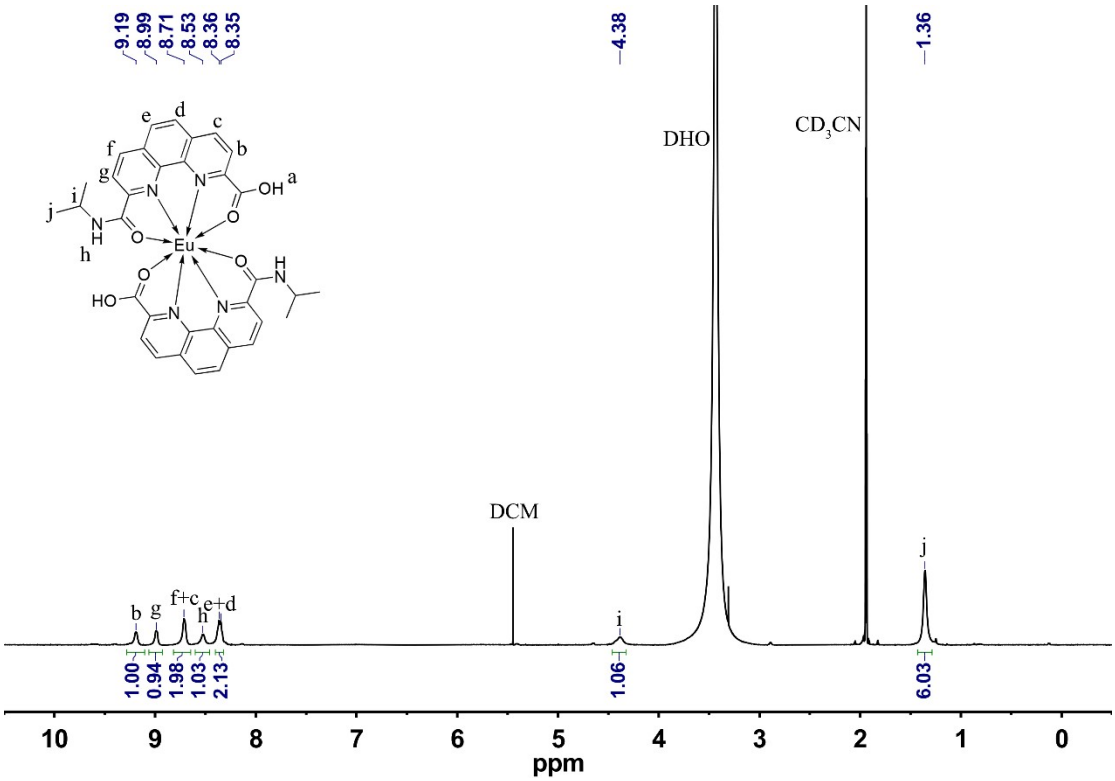

Figure S33. The ^{1}H NMR spectrum of **Eu(6)$_2$** (600 MHz, CD_3CN, 298 K).

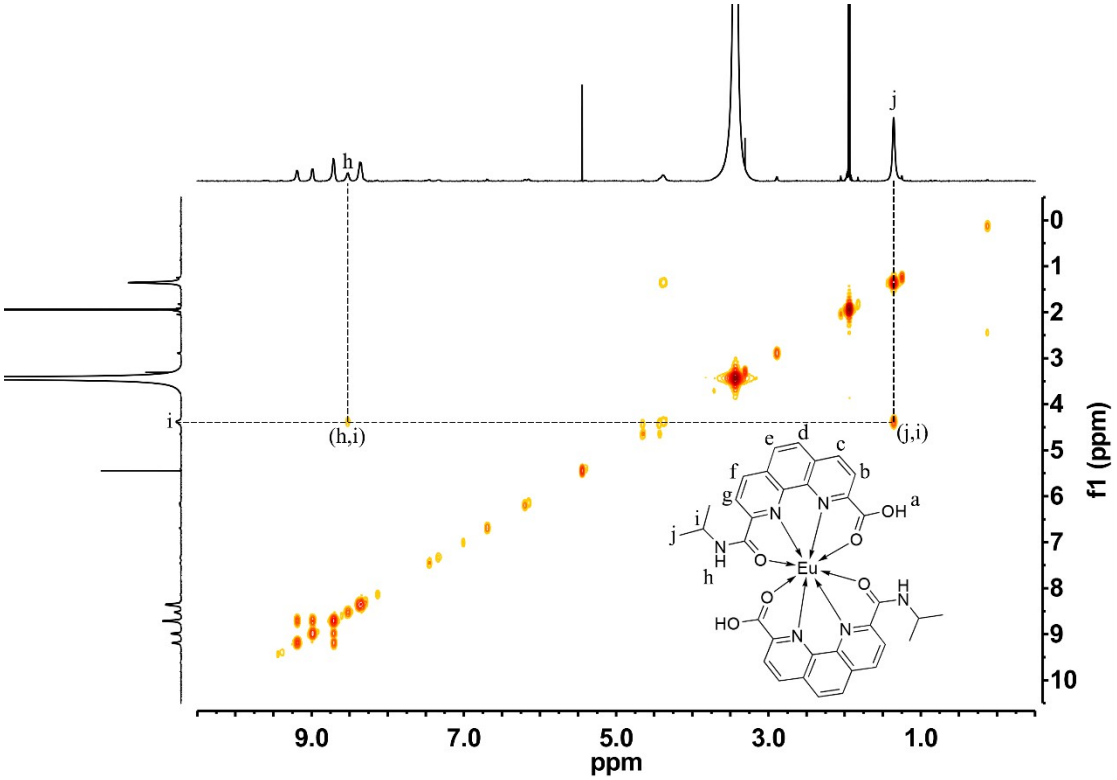

Figure S34. The ^{1}H-^{1}H COSY NMR spectrum of **Eu(6)$_2$** (600 MHz, CD_3CN, 298 K).

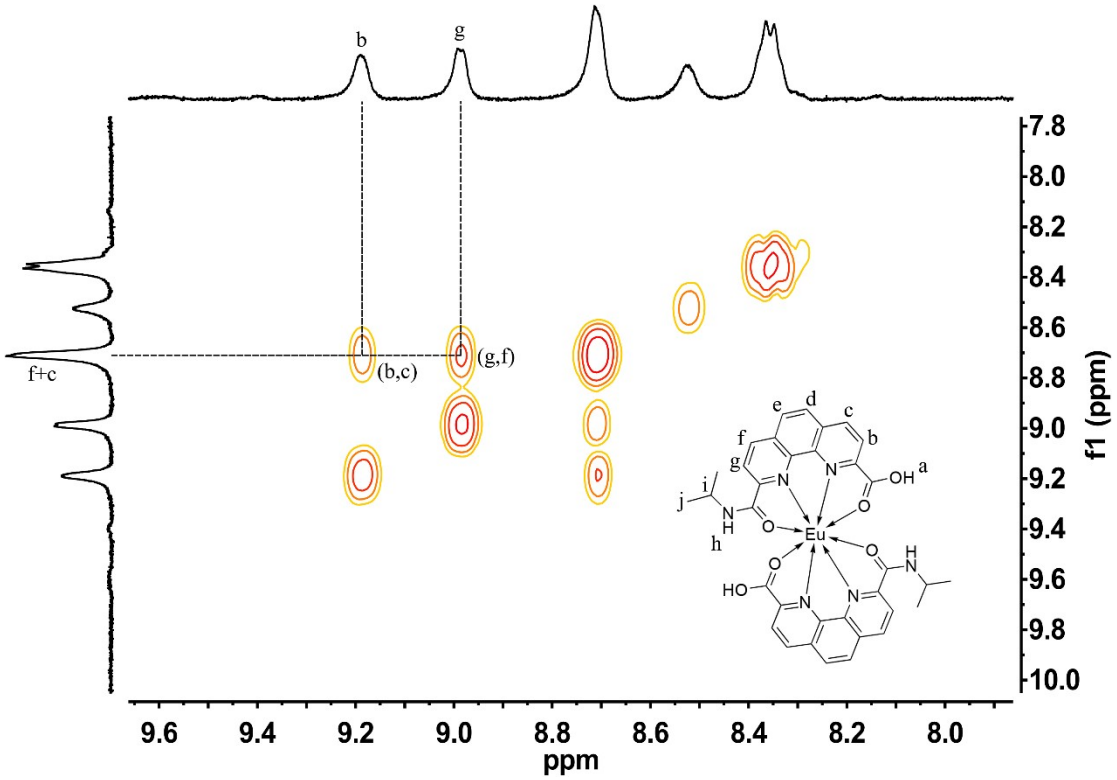

Figure S35. The partial enlargement ^{1}H-^{1}H COSY NMR spectrum of **Eu(6)$_2$** (600 MHz, CD_3CN, 298 K).

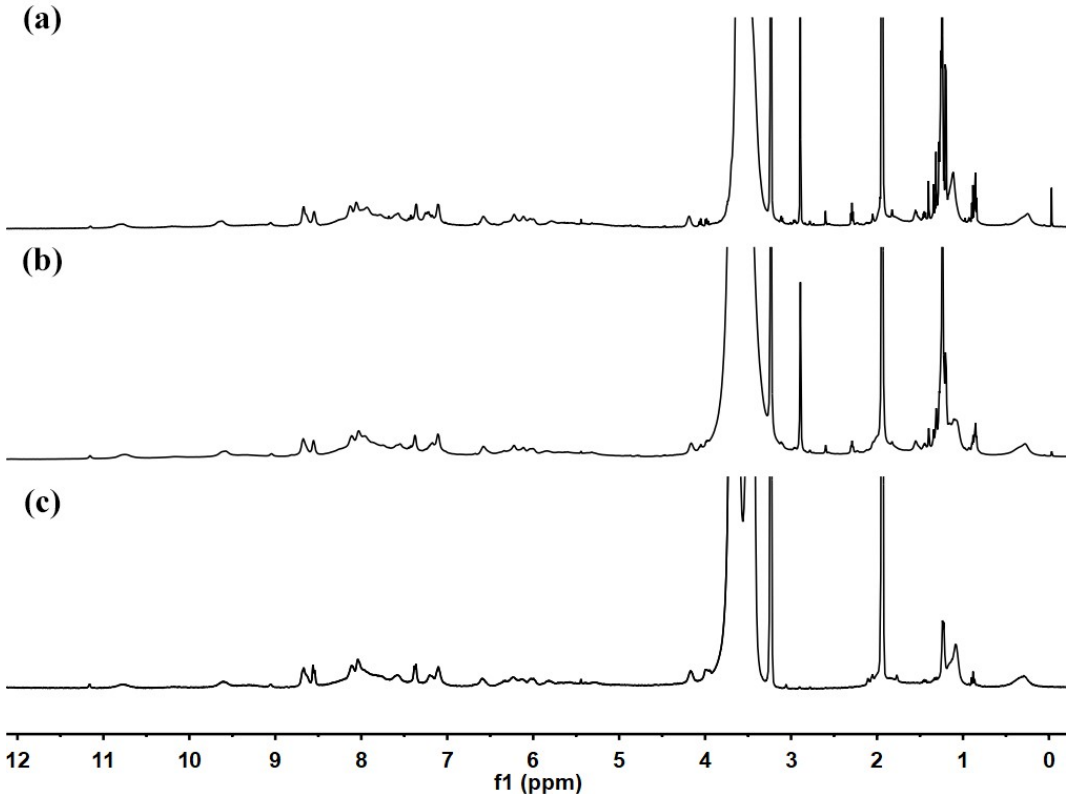

Figure S36. ^{1}H NMR spectra (400 MHz, CD_3CN/CD_3OD v/v = 2/1, 298 K) of $\mathbf{Eu_4L_4}$: (a) after 1 hour of in-situ assembly, (b) after 14 days, and (c) redissolved crystals.

To further investigate the equilibration process, we conducted additional experiments where the NMR tube was sealed and heated for 14 days under the same conditions. As shown in Figure S36, no significant changes in the ^{1}H NMR spectra were observed between the 1-hour and 14-day assemblies, indicating that the system reaches equilibrium within the initial 1-hour timeframe. Furthermore, we measured the 1H NMR spectrum of the complex after dissolving the crystals. The spectrum obtained from dissolved crystals was consistent with that of the assembled complex, further confirming that the NMR behaviour corresponds to the final, equilibrated structure. The broadening of the NMR signals observed in the Eu(III) complex, in comparison to the free ligand, is primarily due to the reduction in symmetry ($C_3 \rightarrow S_4$) and the paramagnetic effects of the Eu(III) ion.

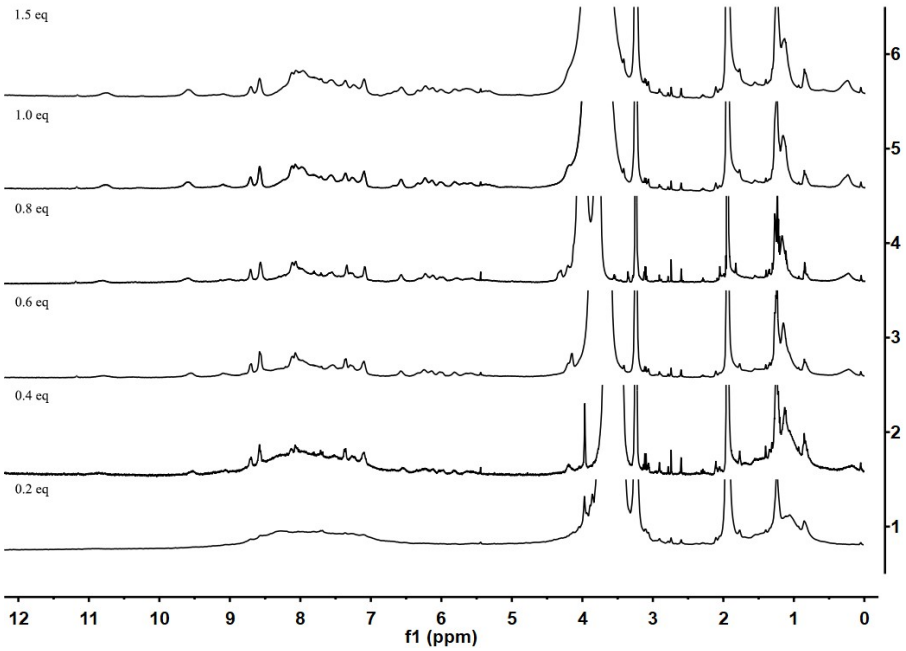

Figure S37 ^{1}H NMR titration spectra (400 MHz, CD_3CN/CD_3OD, v/v = 2/1, 298 K) for the formation of $\mathbf{Eu_4L_4}$, following the addition of different equivalents of $Eu(OTf)_3$ (calculated based on ligand **L**).

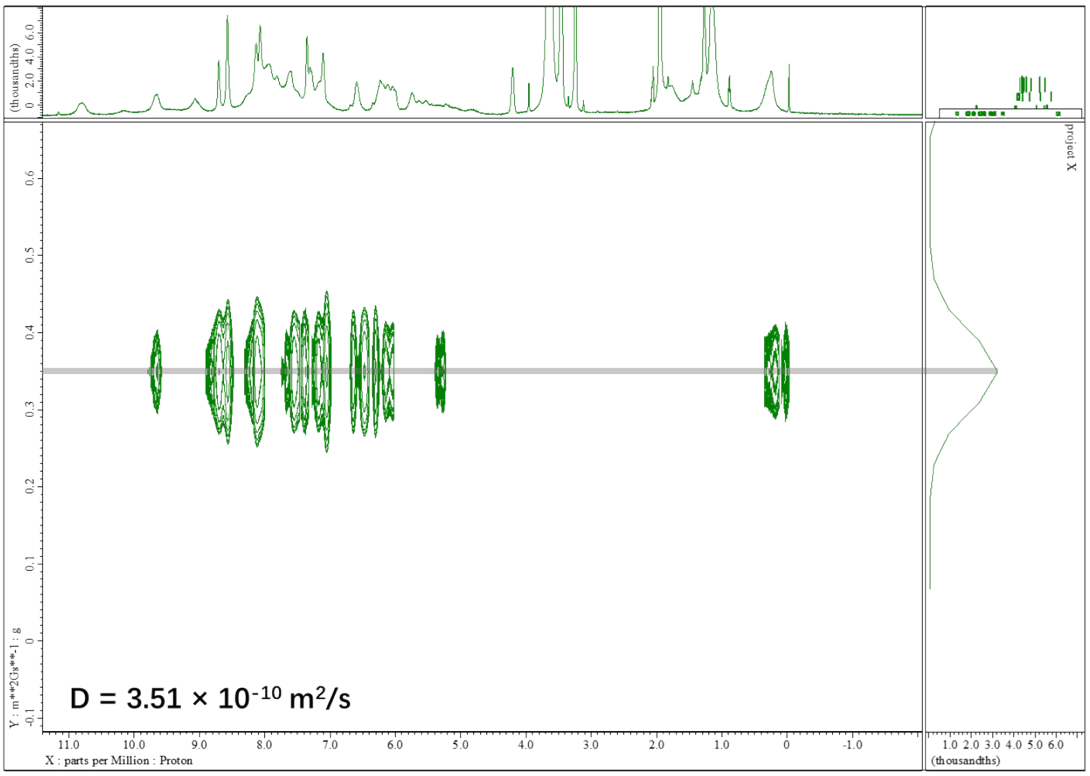

Figure S38. The ^{1}H-^{1}H DOSY NMR spectrum of $\mathbf{Eu_4L_4}$ (600 MHz, CD_3CN/CD_3OD v/v = 2/1, 298 K).

6. Film Preparation

The films are fabricated by spin-coating a solution of **Eu_4L_4** (5 mM in a CH_3NO_2/CH_3OH mixture, v/v = 2/1) onto a glass sheet (1.5 cm × 1.5 cm). The spinning process is conducted for 60 seconds at 3000 rpm.

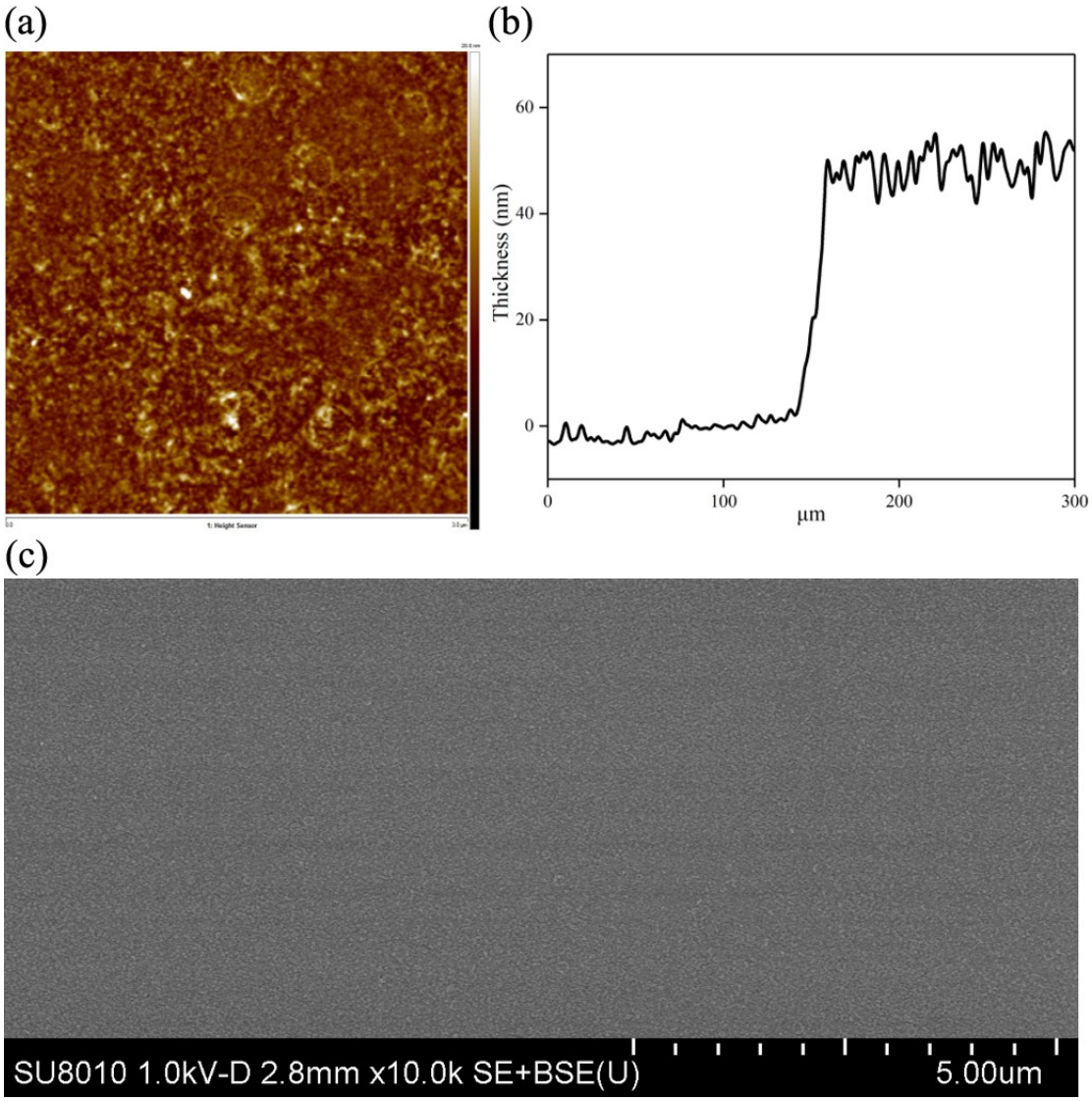

Figure S39. (a) Atomic force microscope (AFM) image, (b) the profilometer characterized result, and (c) scanning electron microscope (SEM) image of the film.

7. Photophysical Properties

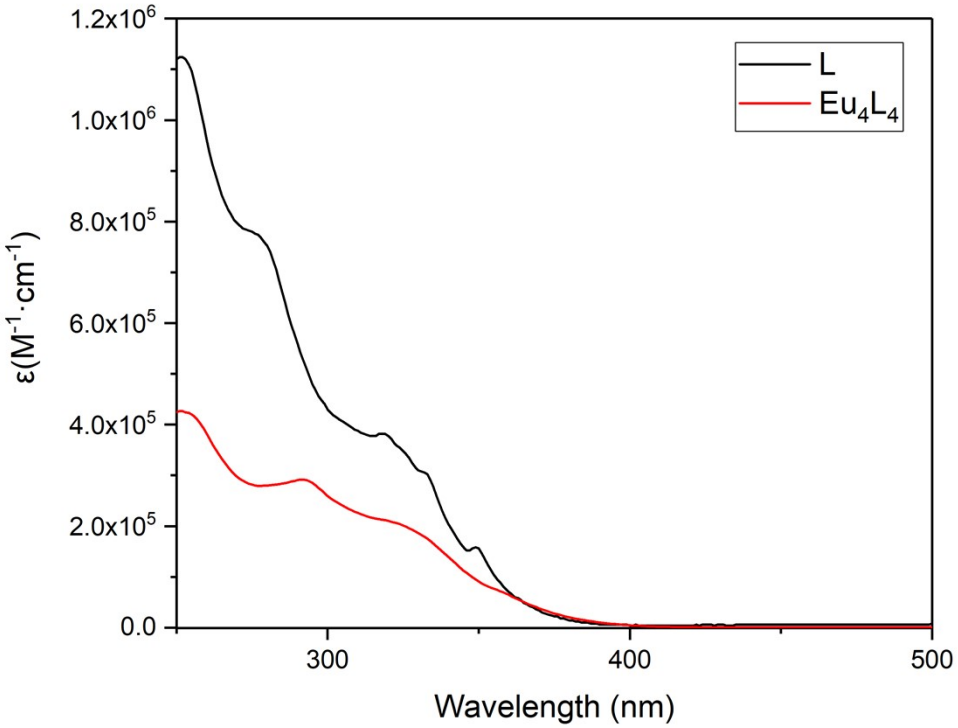

Figure S40. UV-vis spectra of **L** in $CHCl_3$ and $\mathbf{Eu_4L_4}$ in CH_3CN (298 K).

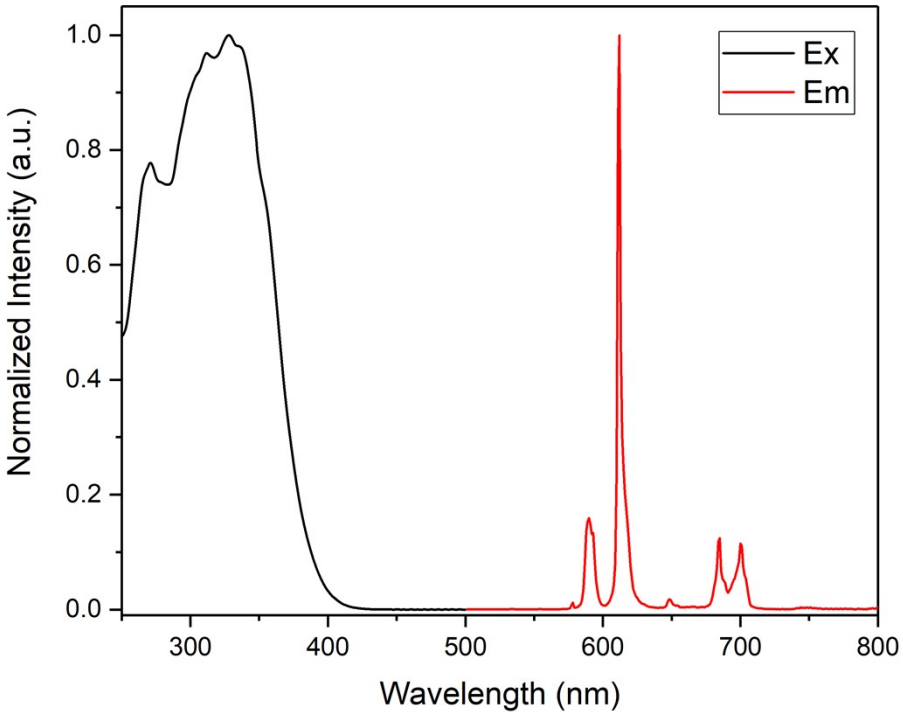

Figure S41. Excitation and emission spectra of $\mathbf{Eu_4L_4}$ in CH_3CN (298 K, c = 5×10^{-6} M).

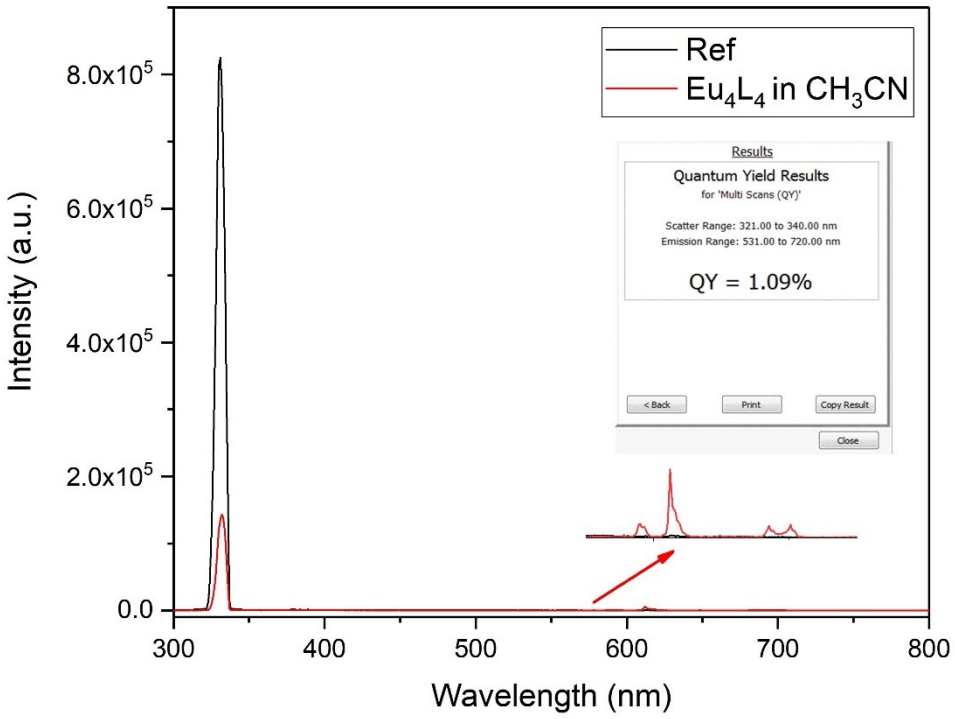

Figure S42. Luminescent quantum yield of **Eu_4L_4** in CH_3CN (298 K, c = 5×10^{-6} M, λ_{ex} = 330 nm).

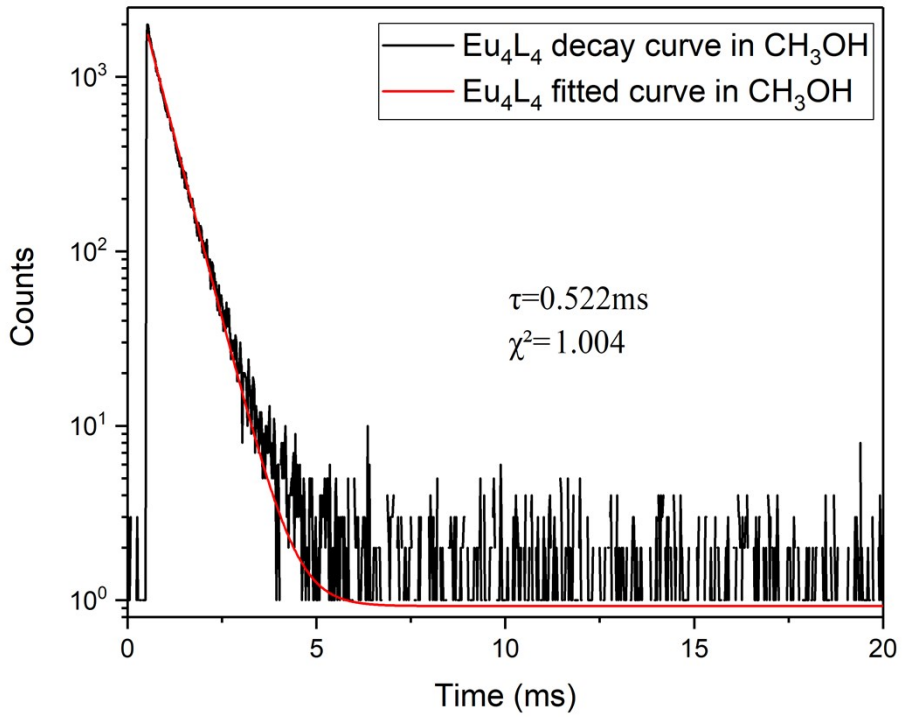

Figure S43. Luminescent lifetimes of **Eu_4L_4** in CH_3OH (c =5×10^{-6} M, λ_{ex} = 330 nm, λ_{em} = 612 nm).

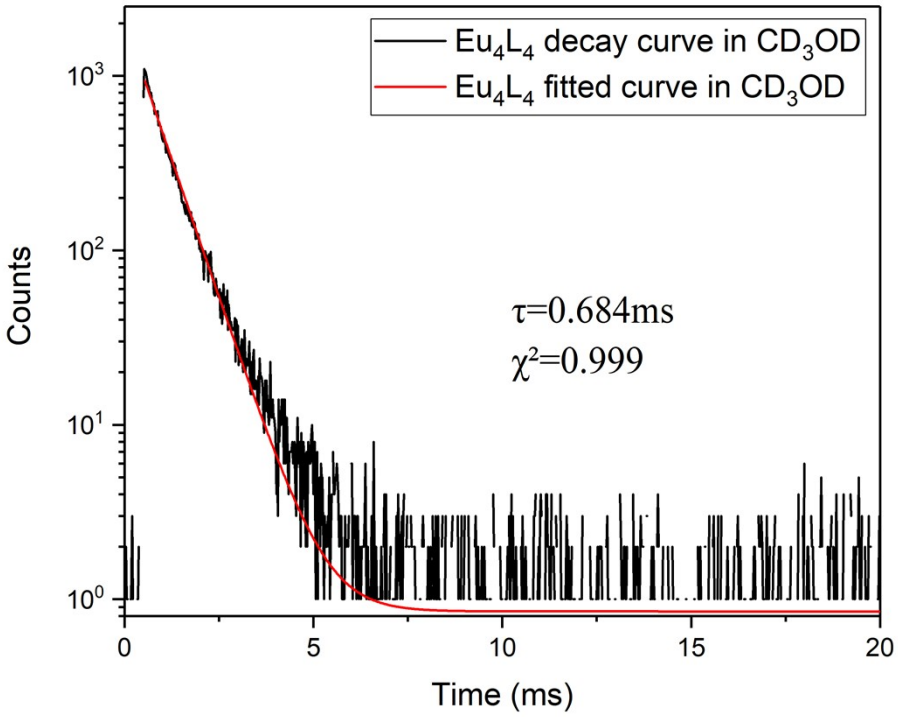

Figure S44. Luminescent lifetimes of **Eu_4L_4** in CD_3OD (c = 5×10^{-6} M, λ_{ex} = 330 nm, λ_{em} = 612 nm).

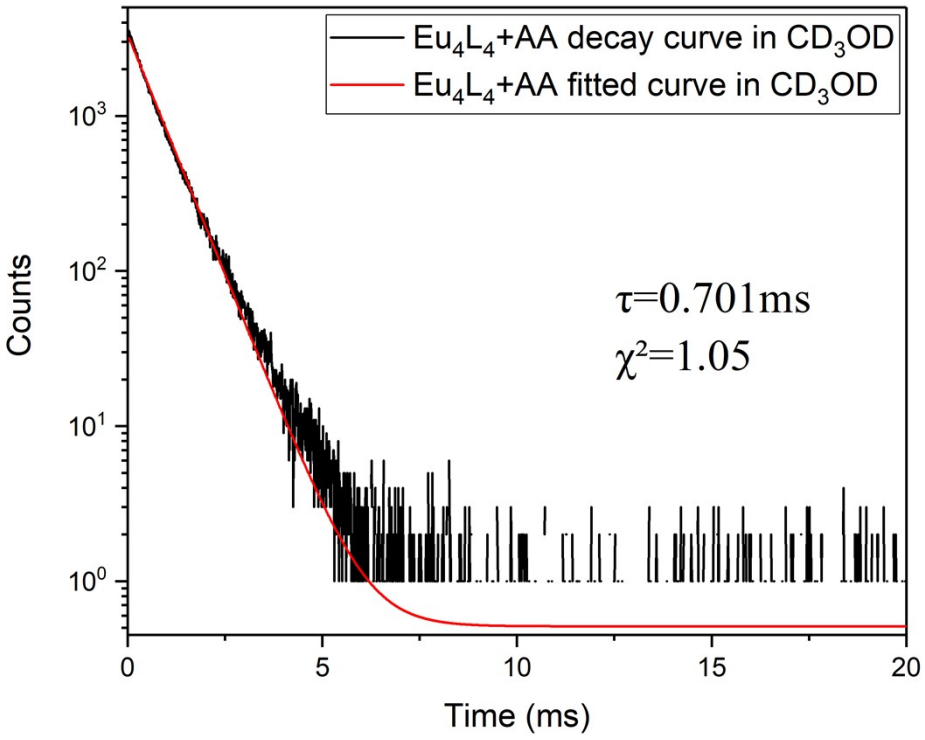

Figure S45. Luminescent lifetime of **Eu_4L_4** in a CD_3OD/AA mixture (v/v = 10:1) at a concentration of 5×10^{-6} M (λ_{ex} = 330 nm, λ_{em} = 612 nm).

The following empirical equation is used to determine the number of solvent molecules q coordinated to Eu^{3+} nodes in **Eu_4L_4** compounds: [S6]

$$q = A\ (\tau_{solvent}^{-1} - \tau_{deutero-solvent}^{-1} - B) \quad (1)$$

Where empirically coefficients A = 2.1 and B = 0 were determined in CH_3OH and CD_3OD conditions. The calculated q value is 0.953 for **Eu_4L_4**, indicating that the metal centres of the cage have about one coordinated solvent molecule.

To further evaluate the potential replacement of coordinated solvent molecules by AA, we measured the luminescence lifetime of **Eu_4L_4** in CD_3OD with excess AA. The calculated number of coordinated solvent molecules (q = 1.027) demonstrates that AA molecules exhibit a negligible ability to replace the solvent molecules coordinated to the $Eu^{(III)}$ centres.

8. Film Responses and Luminescence Enhancement

Preparation of vapours at varying concentrations

Organic vapours of specific concentration were generated by diluting saturated vapours with N_2. Saturated organic vapours were produced by evaporating the organic liquid (trioxymethylene for formaldehyde) in a Schlenk round-bottom flask at 20 ℃ overnight. Subsequently, the saturated vapours were diluted with N_2 using syringes to achieve the desired concentrations.

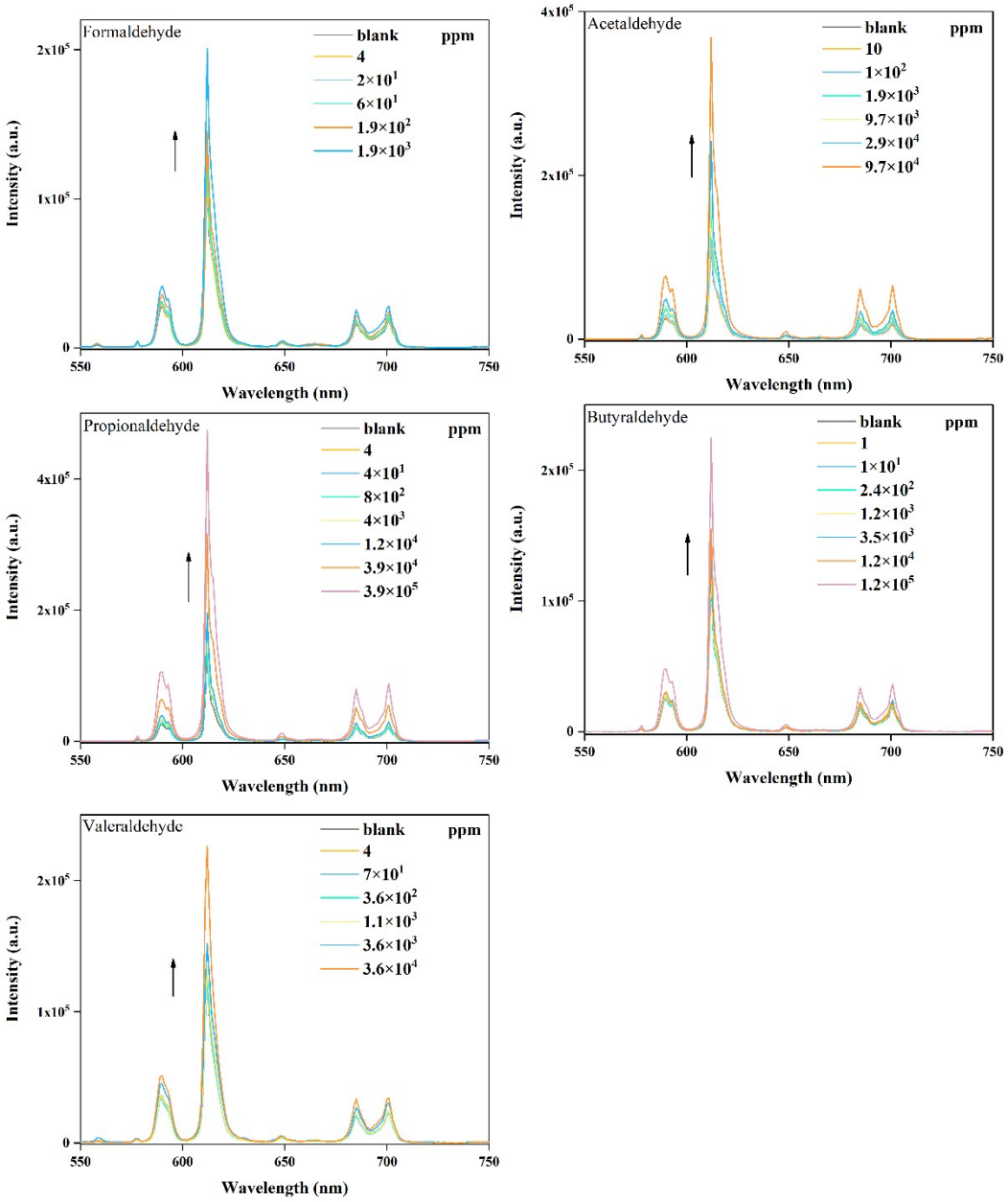

Figure S46. Emission spectra of the Eu_4L_4 films upon exposure to varying concentrations of aldehyde vapours (λ_{ex} = 330 nm).

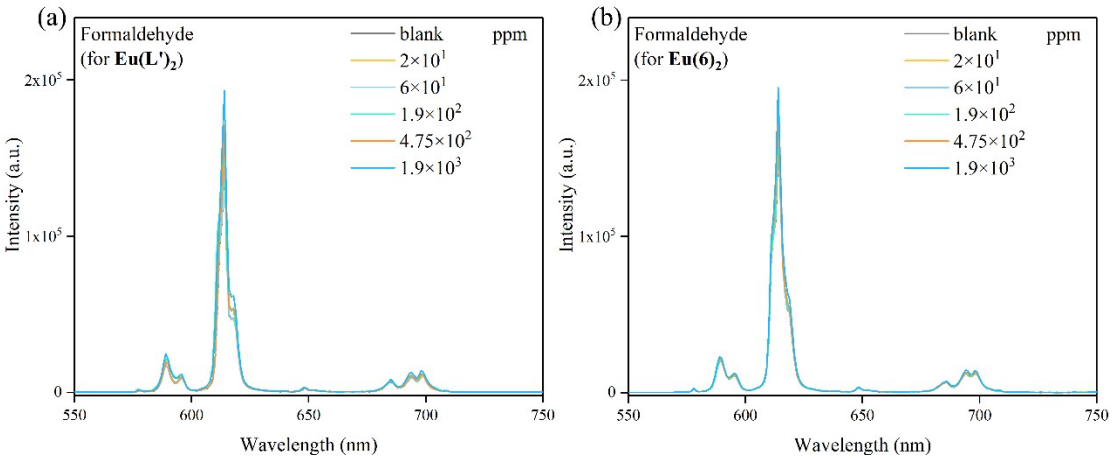

Figure S47. Emission spectra of the **Eu(L')$_2$** (a) and **Eu(6)$_2$** (b) films upon exposure to varying concentrations of FA vapours (λ_{ex} = 336 nm, 338nm respectively).

The overall quantum yield ($\Phi_{overall}$) doesn't adequately reflect the efficiency of the ligand sensitization (Φ_{sens}) or intrinsic quantum yield of europium (Φ_{Ln}). The relationship can be expressed by the following equation: [S7]

$$\Phi_{sens} = \frac{\Phi_{overall}}{\Phi_{Ln}} \quad (2)$$

The intrinsic quantum yields of europium cannot be determined by experimentally due to the weak absorption intensity associated with direct f-f excitation. However, they can be determined by the following two equations: [S7]

$$\Phi_{Ln} = \frac{A_{RAD}}{A_{RAD} + A_{NR}} = \frac{\tau_{obs}}{\tau_{rad}} \quad (3)$$

$$A_{RAD} = \frac{1}{\tau_{rad}} = A_{MD,0} n^3 \left(\frac{I_{tot}}{I_{MD}}\right) \quad (4)$$

Where, A_{RAD} and A_{NR} represent the radiative and non-radiative decay rates, while τ_{obs} and τ_{rad} denote the observed and radiative lifetimes, respectively. The refractive index of the medium is denoted by n, I_{tot} refers to the integrated emission of the $^5D_0 \rightarrow {}^7F_J$ (J = 0 - 4) transition, and I_{MD} corresponds to the integrated emission of the $^5D_0 \rightarrow {}^7F_1$ transition. The spontaneous emission probability for the magnetic dipole transition $^5D_0 \rightarrow {}^7F_1$ is given as $A_{MD,0}$ = 14.65 s^{-1}.

Since, $A_{MD,0}$ and n are not applicable in the film test, these parameters are adjusted by comparing with a blank film in the calculation formula ($\Phi_{Eu}/\Phi_{Eu\text{-}blank}$ and

$\Phi_{sens}/\Phi_{sens\text{-}blank}$).

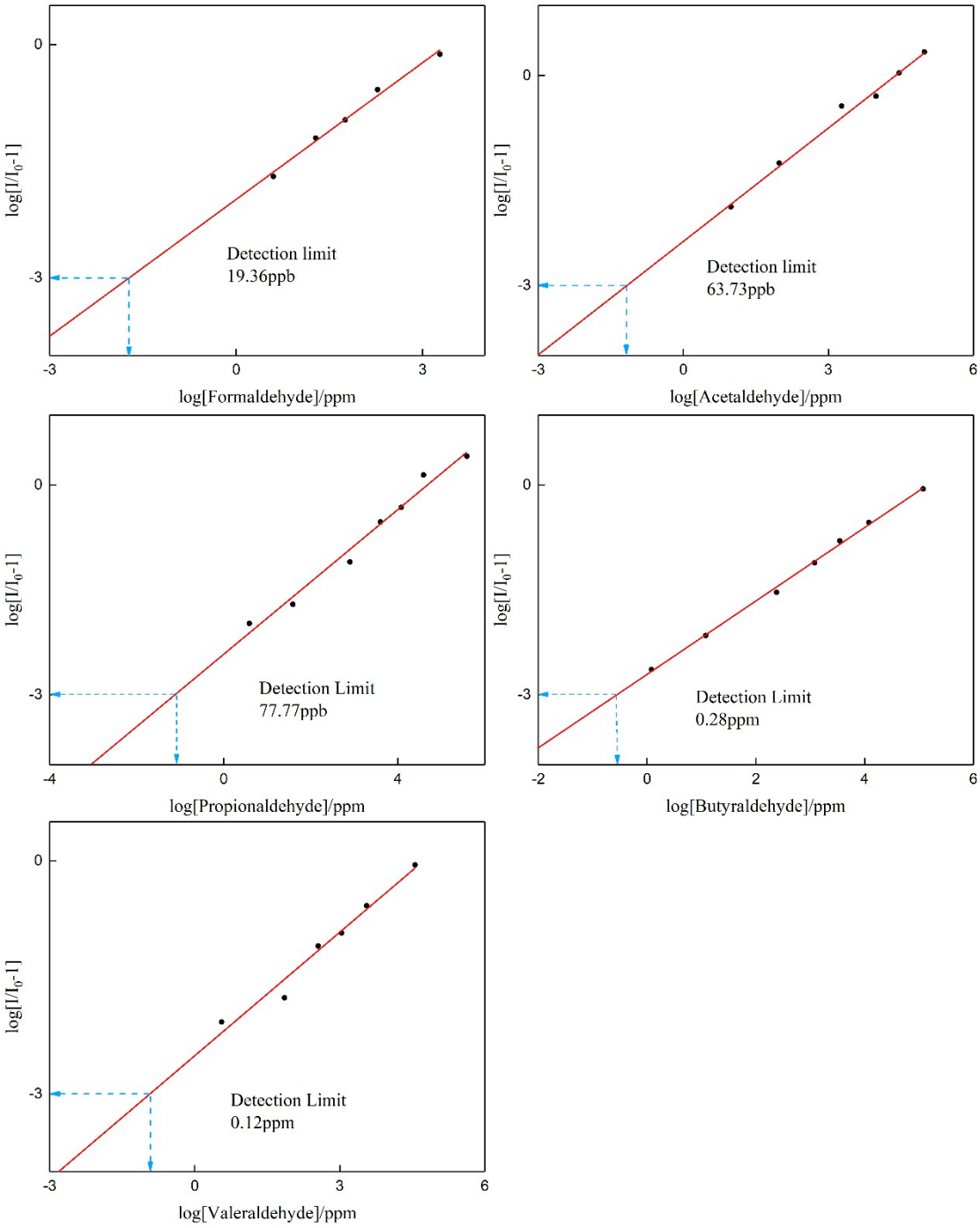

Figure S48. Luminescence enhancement efficiency (I/I_0-1) of the $\mathbf{Eu_4L_4}$ film as a function of the vapour concentration for various aldehydes.

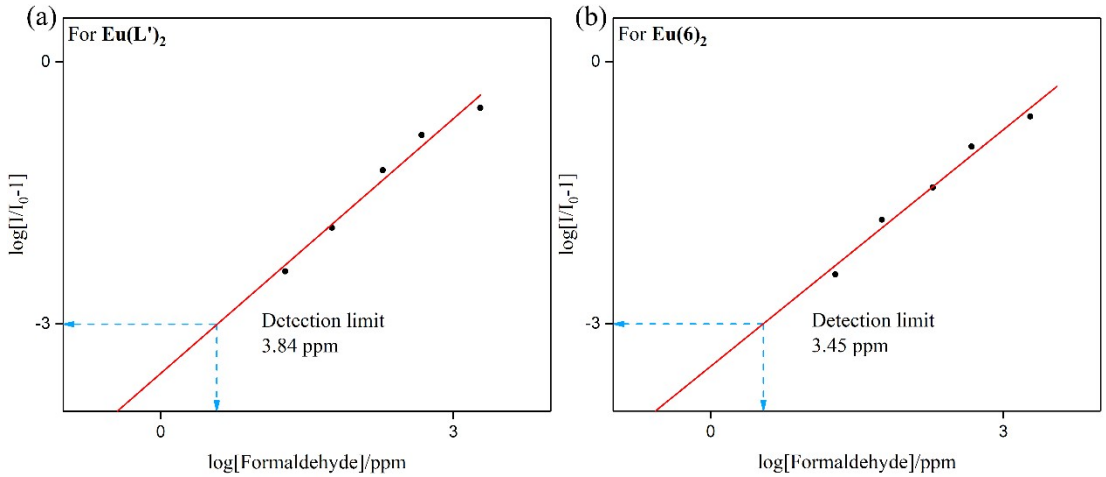

Figure S49. Luminescence enhancement efficiency (I/I_0-1) of the **Eu(L')$_2$** (a) and **Eu(6)$_2$** (b) film as a function of the vapour concentration for FA.

Eu$_4$L$_4$ films achieved a detection limit of 19.4 ppb, which is only 0.5% of the detection limit of **Eu(L')$_2$** and **Eu(6)$_2$** films (19.4 ppb vs. 3.8 ppm and 3.5 ppm). This highlights the significantly higher sensitivity of **Eu$_4$L$_4$** films compared to their mononuclear counterparts.

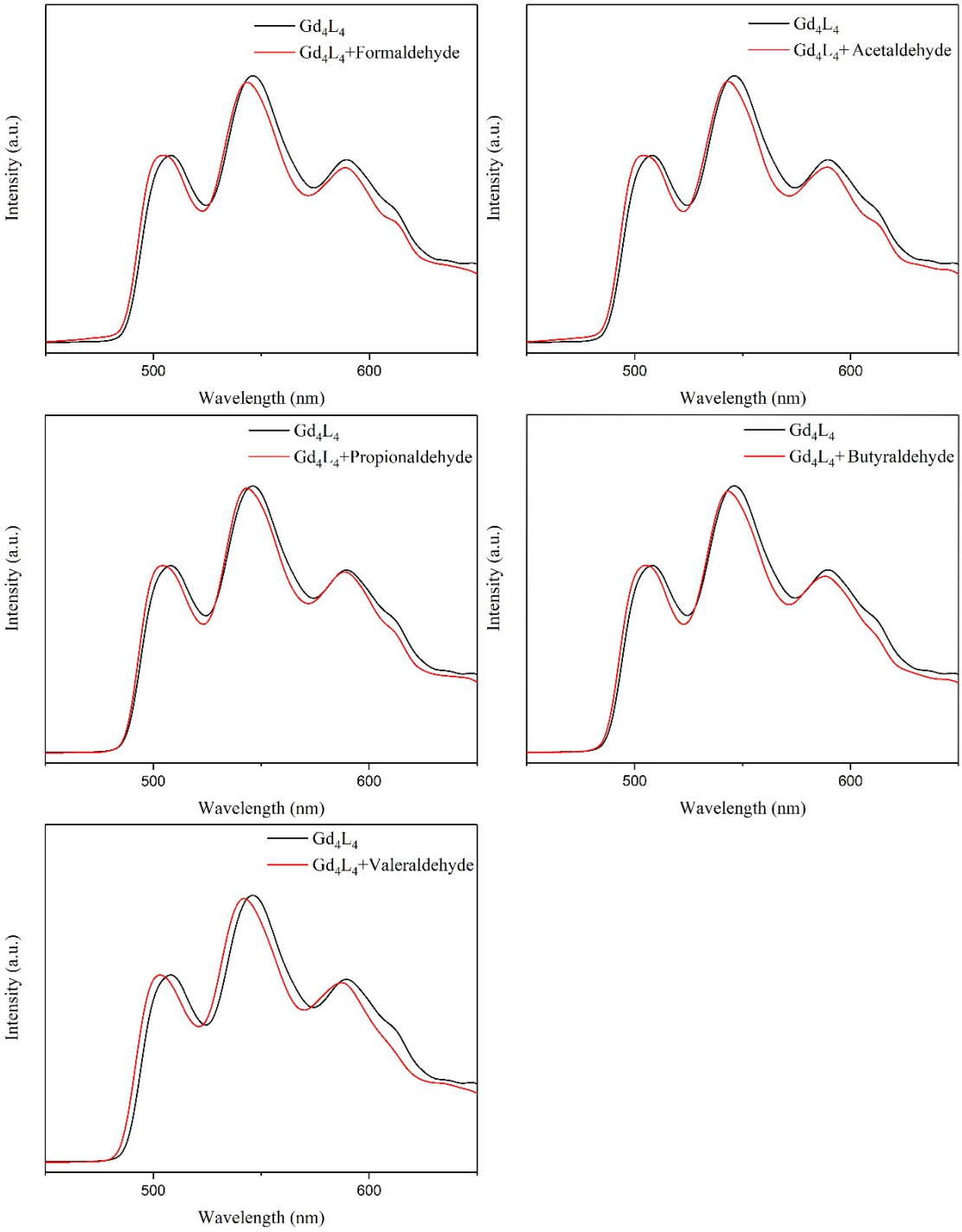

Figure S50. Phosphorescence emission spectra of **Gd_4L_4** in CH_3CN ($c = 1.7\times10^{-6}$ M) upon the addition of various aldehydes.

9. Supplementary References

[1] M. Yamamura, T. Saito and T. Nabeshima, *J. Am. Chem. Soc.*, **2014**, *136*, 14299-14306.

[2] Y. Yang, T. K. Ronson, Z. Lu, J. Zheng, N. Vanthuyne, A. Martinez and J. R. Nitschke, *Nat Commun*, **2021**, *12*, 4079.

[3] C. Jiang, S.-J. Hu, L.-P. Zhou, J. Yang and Q.-F. Sun, *Chem. Commun.*, **2022**, *58*, 5494-5497.

[4] J. B. Maglic, R. Lavendomme, *J. Appl. Cryst*. 2022, 55, 1033–1044.

[5] L. Farrugia, *J. Appl. Cryst.*, **2012**, *45*, 849-854.

[6] R. C. Holz, C. A. Chang and W. D. Horrocks, *Inorg. Chem.*,1991, 30, 3270–3275.

[7] X. Q. Guo, L. P. Zhou, L. X. Cai and Q. F. Sun, *Chem.-Eur. J.*, **2018**, *24*, 6936-6940.